Comparative Evaluation of Anticancer Efficacy and Molecular Mechanism of Silver Nanoparticles Synthesized from Methanolic and Ethanolic Extracts of Citrus medica

Ejaj Ahmad
Govind Ballabh Pant Institute of Postgraduate Medical Education and Research: Govind Ballabh Pant Hospital

Mohammed Sajid
NICPR: National Institute of Cancer Prevention and Research

Alina Athar
Govind Ballabh Pant Institute of Postgraduate Medical Education and Research: Govind Ballabh Pant Hospital

Arun Kumar
Govind Ballabh Pant Institute of Postgraduate Medical Education and Research: Govind Ballabh Pant Hospital

Nimisha Nimisha
Govind Ballabh Pant Institute of Postgraduate Medical Education and Research: Govind Ballabh Pant Hospital

Abhay Kumar Sharma
Govind Ballabh Pant Institute of Postgraduate Medical Education and Research: Govind Ballabh Pant Hospital

Mohammad Zulfazal Ahmed
King Saud University

Ali Saeed Alqahtani
King Saud University

Mausumi Bharadwaj
NICPR: National Institute of Cancer Prevention and Research

Sundeep Singh Saluja
sundeepsaluja@yahoo.co.in

Govind Ballabh Pant Institute of Postgraduate Medical Education and Research: Govind Ballabh Pant Hospital

Research Article

Keywords: Citrus medica, Green synthesis, Silver nanoparticle, Anticancer, MCF-7

Posted Date: April 18th, 2025

DOI: https://doi.org/10.21203/rs.3.rs-5826386/v1

Version of Record: A version of this preprint was published at Journal of Materials Science: Materials in Engineering on October 15th, 2025. See the published version at https://doi.org/10.1186/s40712-025-00285-w.

Abstract

The development of biosynthesized and cost-efficient nanomedicine is a promising strategy in cancer therapeutics. Herein, we have synthesized highly potent silver nanoparticles (AgNPs) using methanolic and ethanolic extracts of *Citrus medica* fruit, unraveling the significance of different solvents. Fourier transform Infrared spectroscopy confirmed the occurrence of secondary metabolites on the synthesized AgNPs' surface. The Zetasizer analysis showed no significant particle-size differences between both solvents based-synthesized AgNPs; however, zeta potential showed significant differences in the particle surface charge. The high-resolution transmission electron microscopy confirmed a predominantly spherical morphology of AgNPs. Notably, AgNPs synthesized from ethanolic extracts exhibited smaller sizes (5-7 nm) and a more uniform distribution compared to their methanolic counterparts. The X-ray diffraction demonstrated a polycrystalline nature with a face-centered cubic structure. Functional assays showed a significant increase in the anticancer efficacy of ethanolic extract-derived AgNPs against the breast cancer cells (MCF-7 and MDA-MB-231), accompanied by extensive DNA fragmentation and enhanced induction of apoptosis. Mechanistically, both methanolic and ethanolic AgNPs induce upregulation of pro-apoptotic gene expression (e.g., *TP53*, *BAX*, and *CYCS*) and downregulation of anti-apoptotic gene (e.g., *BCL2*). The flow cytometry analysis showed a substantial increase of the ethanolic extract-based AgNPs in the late-stage apoptotic cells, which was further confirmed by morphological changes in treated MCF-7 cells. This study reveals the pivotal influence of the selection of solvent on the synthesis and anticancer potency of AgNPs, significantly impacting their ability to induce apoptosis in MCF-7 cells. Our findings introduce a novel strategy for optimizing green synthesized AgNPs-based therapies, offering promising avenues for advancing nanoparticle-driven cancer treatments and potentially transforming future therapeutic approaches in oncology.

Highlights

- To analyze the role of organic solvent-based extraction of phytochemicals and their influence on the physiochemical properties of the synthesized AgNPs.
- Assessment of the anticancer efficacy of methanolic or ethanolic extracts of *Citrus medica* fruit-based synthesized AgNPs on MCF-7 cells.
- The synthesized AgNPs induce apoptosis through an increased expression of pro-apoptotic genes (*BAX*, *p53*, and *CYCS*) and reduced expression of the anti-apoptotic gene (*BCL2*).
- AgNPs synthesized through ethanolic extract more effectively induce apoptosis in MCF-7 cells.

1. Introduction

Breast cancer (BC) falls among the cancers that are associated with a high mortality rate globally and causes 6.9% of all cancer-related deaths (Sung et al. 2021; Bray et al. 2024) The early stage of BC diagnosis would enable a complete cure of the disease. However, due to the lack of visible symptoms at an early stage, the disease is mainly diagnosed at a late stage, leading to a high death rate among

cancer patients. The treatment modalities primarily include traditional approaches like surgery, chemotherapy, and radiotherapy. Chemotherapy kills most cancer cells; however, long-term exposure to chemotherapeutics promotes the origin of cancer stem cells (CSC), leading to the development of new cancer cells. These cells create a huge huddle in BC treatment owing to the development of resistance to chemotherapeutic agents, which plays a pivotal role in propagation, recurrence, and metastasis (Nahvi et al. 2022) Thus, strategies need to be adopted to minimize exposure to CSC to anticancer drugs to prevent the development of drug-resistant cells.

Nanomedicine has immense potential for BC treatment by minimizing the long-term exposure of the anticancer drugs to the cells by encapsulating them into nanocarriers that release a limited quantity of drugs in a sustained fashion. Thus, numerous innovative approaches have been designed that led to the development of new nanocarriers or ligands decorated nanocarriers in which anticancer drugs were encapsulated, and their efficacy has been analyzed against BC cell lines and xenograft tumors in animal models (Tagde et al. 2022; Rahman et al. 2023) Moreover, some commercial nanomedicines, such as Doxil and Abraxane, were developed against BC. These nanomedicines are now used as adjuvant therapy against BC and show favorable clinical outcomes (Wu et al. 2017; Jiang et al. 2022). However, these nanomedicines are expensive and cause some form of toxicity in healthy cells.

The development of non-toxic and economical nanomedicine hunt led to the exploration of novel metallic nanoparticle potential that includes the use of metals like Au, Ag, Pt., etc. These metallic nanoparticles have shown utility in various fields and exhibit efficacy against cancer cells. The high efficacy of metallic nanoparticles against cancer cells is due to their small size distribution, shape, long-term activity, and capability to exhibit optical and magnetic properties (Khan et al. 2017). Metallic nanoparticles are readily uptake by the cells owing to their high density, which could help in the management of cancer (Odularu 2018; Sharma et al. 2018). Among the metallic nanoparticles, the attributes of silver metal-based nanoparticles exhibited exceptional characteristics including exceptional physio-chemical, and biological properties, which makes them unlike their macroscale counterparts (Sharma et al. 2009).

Moreover, silver is a non-toxic metal/element that shows high electrical and thermal conductivity as well as stability at ambient temperature. Also, it displays a wide array of absorption of visible and far IR regions, surface-enhanced Raman scattering, chemical stability, and nonlinear optical behaviours (Zhang et al. 2016; Chouhan 2018; Jain et al. 2021). These properties of silver metal made it more valuable than other metallic nanoparticles. However, silver nanoparticles prepared by physical and chemical methods may contain harsh and unfriendly environmental compounds and solvents that cause toxicity (Kharissova et al. 2019). Thus, an alternative nanoparticle synthesis method was envisioned, which led to the development of the green synthesis of metallic nanoparticles. The approach overcame some problems associated with physical and chemical methods of metallic nanoparticle toxicity.

The green synthesis of silver nanoparticles uses various parts of plants, algae, and micro-organisms, which contain phytochemicals/secondary metabolites and compounds containing functional groups

such as aldehyde, alcohol, and ketone, which causes the reduction of Ag^{+} to Ag^{0} (Zuhrotun et al. 2023). The chain propagation led to the synthesis of AgNPs. Further, these secondary metabolites cause the stabilization and capping of AgNPs. The prepared AgNPs are economical and eco-friendly. The extraction of compounds from the plants or their parts depends on the nature of the solvents owing to the physiochemical properties of the phytochemicals present in the plant (Bitwell et al. 2023). AgNPs were synthesized by extracting the phytoconstituents of plants and their parts in various organic solvents, and their anticancer/biological properties were evaluated (Das et al. 2013; Chitsazi et al. 2016; Heidari et al. 2018; Antropova et al. 2021). The synthesized AgNPs showed effective anticancer properties against some cancer cell lines (Das et al. 2013; Heidari et al. 2018). Kis et al. synthesized AgNPs from ethanolic extract of *Populae gemmae* extract and observed a significant decrease in the growth of MCF-7 and A549 cancer cell lines (Kis et al. 2022). *Citrus medica* (Citron), is a big and rough-surfaced lemon-like fruit belonging to the family Rutaceae (Davidson 2006). The extensive research focus on its antipathogenic capabilities undoubtedly stems from its remarkable abundance of phytochemicals known for their potent antimicrobial effects (Benedetto et al. 2023).

Herein, we have prepared AgNPs from methanolic and ethanolic extracts of *Citrus medica* fruit separately and characterized them through various biophysical techniques. The anticancer efficacy of these formulations was checked on the breast cancer cells (MCF-7) to comprehend the influence of solvent in the extraction of secondary metabolites from the fruit and their influence in the synthesis of AgNPs. Further, the molecular mechanisms of cancer cell growth inhibition of these AgNPs treated cells were evaluated by DNA fragmentation analysis and quantification of proapoptotic, anti-apoptotic, proto-oncogene of the cell cycle, mitochondria, as well as tumor suppressor gene by real-time PCR.

2. Material and Methods

2.1. Material

The *Citrus medica* (Citron) fruit was procured from the local market of Lucknow, Uttar Pradesh, India. Reagents, such as SulforhodamineB (SRB), 2, 2-Diphenyl-1-picrylhydrazyl (DPPH), Silver nitrate, and Potassium bromide procured from Sigma Aldrich (Sigma-Aldrich Chemicals Pvt. Ltd., Bangalore, India). Penicillin, Gentamycin, Streptomycin, DMEM/F-12, trypsin-EDTA (0.5%), FBS, and Verso cDNA synthesis kit were obtained from Thermo Scientific (Waltham, MA). Methanol and ethanol were purchased from Qualigen Fine Chemicals, Maharashtra, India. Milli Q and distilled water were prepared in the Laboratory, using the Millipore purification system. A breast cancer cell line (MCF-7) was obtained from ATCC whereas MDA-MB-231 was procured from the NCCS, Pune, India and other chemicals used that are not mentioned were also of analytical grade.

2.2. Methods

2.2.1. Silver nitrate ($AgNO_3$) solution preparation

Silver nitrate solution (10 mM) was prepared in Milli-Q water under a magnetic stirrer for 2 hr, and the solution was further filtered with Whatman paper no.1 to remove any impurities. The prepared solution was kept in an amber-coloured reagent bottle to avoid photodecomposition of $AgNO_3$.

2.2.2. Methanolic and ethanolic *Citrus medica* fruit extract preparation

The *Citrus medic*a fruit was cleaned thoroughly in running water followed by rinsing with Milli-Q water. Then, it was dried in a hot air oven under controlled 45–50℃ for 48 hr. Next, the fruit was chopped into small pieces using a surgical blade and further dried at the same temperature for 24 hr. Subsequently, dried fruit was made into fine powder by mortar and pestle. Then, 50 mL of methanol and ethanol (70%) were added into 5 g (10% w/v) of each dried power in a separate Erlenmeyer flask and kept overnight (in the dark) at room temperature. Next, the prepared mixtures (10% w/v) were sonicated using a sonicator (Branson CPX5800H, Richmond, VA) for 1 hr and passed through a Whatman filter paper (Grade-1). The filtrates were stored at 4℃ and used (within two weeks) to synthesize AgNPs.

2.2.3. Biosynthesis and isolation of AgNPs from methanolic and ethanolic extract

The solubility of biochemical compounds depends on the polarity of the solvent. Thus, we have extracted the secondary metabolites/phytochemicals of *Citrus medica* fruit in two different organic solvents *viz.* methanol and ethanol (70% v/v) that were used to synthesize AgNPs.

For methanolic extract-based green synthesis of silver nanoparticles (Met-AgNPs), we have prepared (10% w/v) methanolic extract of *Citrus medica* fruit. The influence of different parameters such as concentration of $AgNO_3$ solution, the quantity of extract, temperature, pH, rotation (rpm), and incubation time was carefully evaluated to prepare small-size AgNPs. After varying each parameter, the UV-Vis spectrum of the reaction mixture was analyzed to ascertain whether nanoparticles were synthesized or not. Once we got the designated peaks of the reaction mixture, then subsequently, the size of the particles was analyzed using Zetasizer. By varying these parameters, we successfully synthesized the smallest size of AgNPs when 10 mM of 30 mL $AgNO_3$ and 1 mL of extract (30: 1) were allowed to continuously rotate at 500 rpm at 70ºC for 2 hr on a magnetic stirrer (Daihan Scientific, South Korea). A gradual time-dependent change of colour from a colourless solution to pale yellow and then light brown was observed. However, a distinct brown colour appeared after 1 hr. This optical colour change advocates that biomolecules/secondary metabolites present in the *Citrus medica* fruit extract reduced the silver ions into AgNPs.

Similarly, the smallest size of AgNPs was prepared from the ethanolic extract (Eth-AgNPs) by varying the parameters mentioned above. We could prepare the smallest size of Eth-AgNPs from the same ratios of $AgNO_3$ and ethanolic *Citron* fruit extract, temperature, and rotation. However, the Eth-AgNPs are formed at lower $AgNO_3$ solution (1 mM) and require a longer duration *viz.* 2 hr. A gradual colour change of the solution (from light brown to dark brown) was observed within 2 hr time which suggests AgNP synthesis

owing to the reduction of $Ag^{+} \rightarrow Ag^{\circ}$ by secondary metabolites of fruit extract. The biosynthesized AgNPs were separated by centrifugation for 10 min at 13,500x g by a centrifuge (Eppendorf, Hamburg, Germany). The AgNPs pellet was washed three times with MQ water. Then, the isolated AgNPs were dried by placing them into a vacuum oven at 45ºC, 0.8 bar (Daihan Scientific, South Korea) for 2 hr and froze at -80ºC until further applications.

2.2.4. Biophysical characterization of synthesized AgNPs

For the characterization (size, shape, and charge) of prepared AgNPs various techniques were used including UV-Vis spectroscopy, FTIR, Zetasizer, XRD, and TEM imaging. Initially, the UV-Vis spectra of the Met-AgNPs and Eth-AgNPs were acquired by adding the 200 µL of the formulations in microtiter plate wells and scanned from 300 to 700 nm range with 1 nm resolution through a multimode reader (VarioSkan Lux, Thermo-scientific, USA). Next, the FTIR spectra of the Met-AgNPs and Eth-AgNPs ere were scanned within a wavelength 4000 – 500 cm^{-1} range with 1 cm^{-1} spectral resolution (Brucker, Optika GmbH, Karlsruhe, Germany). Further, the Met-AgNP's size (average), polydispersity index (PDI), and zeta potential were determined (at 25ºC temperature) by the Malvern Zetasizer Pro Blue instrument (Malvern Analytical Ltd, Malvern UK). To comprehend the phase and crystalline structure of the Met-AgNPs and Eth-AgNPs, an XRD pattern was noted using a Rigaku D/Max-IIIC diffractometer applying CuKα monochromatic radiation and AXIS Supra by a monochromatic source (Al anode Kα: 1486.6eV) between 2θ of 10 to 80°. TEM images of either Met-AgNPs or Eth-AgNPs AgNPs were acquired to analyze their actual sizes and morphologies. Before imaging, the samples were sonicated (5 min) in a sonicator (Branson, 5800). The respective AgNPs (100 µL) were added to Milli-Q water (900 µL), and samples (5 µL) were gently positioned on a carbon-coated copper grid and samples were dried in the air using a lamp heat. The TEM evaluation of both AgNPs was accomplished at an accelerating voltage of 200 kV (FEI Tecnai G^2 20 S-Twin).

2.2.5. Analysis of antioxidant activity

The antioxidant action of *Citrus medica* fruit extracts (methanolic/ethanolic) and their respective extract-based AgNPs (Met-AgNPs and Eth-AgNPs) was determined by DPPH assay (Bhakya et al. 2016). Briefly, 100 µL of different concentrations of extracts and synthesized AgNPs prior dissolved in 80% ethanol solution were added into 96 well plates (in triplicate). Varying concentrations of ascorbic acid (100 µL) were used as a positive control. Afterward, 0.2 mM DPPH reagent was prepared in ethanol (80%) and added to each well. The plate was incubated for 30 min (no light exposure) at room temperature and the plate was read at 517 nm by a multimode reader (VarioSkan Lux, Thermo-scientific). The free radical scavenging activity was determined by the below-mentioned equation.

$$\text{DPPH free radical scavenging activity } = \frac{\text{Abs (control)} - \text{Abs (sample)}}{\text{Abs (control)}} \text{ X } 100$$

2.2.6. Evaluation of Anticancer Analysis

2.2.6.1. Analysis of antiproliferative activity against breast cancer cells

To measure the cytotoxic activity of Met-AgNPs and Eth-AgNPs, the SRB assay was accomplished as defined earlier by Vichai et. al. 2006 with few changes (Vichai and Kirtikara 2006). The cells (MCF-7/MDA-MB-231) were seeded (10^4 cells/well) in culture plates (96 wells) and incubated in a CO_2 incubator for 24 and 48 hr at 37ºC. The DMEM medium was replaced with fresh medium (100 µl/well) and different concentrations of either Met-AgNPs or Eth-AgNPs ranging from 3.125 to 100 µg/mL prepared in DMEM medium were supplemented to the corresponding wells in triplicates. After incubation (24 and 48 hr), the cells were washed with PBS and fixed using Trichloroacetic acid (10%) for 1 hr at 4ºC. Then, the plates were washed four times with sterile distilled water and dried. The 100 µL of SRB solution (0.057%) was added for 30 min at room temperature. The plates were immediately rinsed four times with acetic acid (1%) and kept for drying at room temperature. Finally, 10 mM Tris base buffer (pH 10.5) was added (200 µL/well) to the wells, and absorbance at 564 nm was taken by a microplate reader (SPECTROstar Nano, BMG Labtech, Ortenberg, Germany).

2.2.7. Analysis of DNA fragmentation

MCF-7 cancer cells were grown on 6 well plates and incubated with IC_{50} of AgNPs for 24 hr. Later, the cells were harvested after washing with PBS, and collected in the microcentrifuge tube by centrifuging at 4000xg for 5 min. The lysis buffer (600 µL/tube) comprising Tris-HCl (10 mM, pH-7.4), NaCl (400 mM), EDTA (100 mM), and SDS (6%) was added to the tubes. Then, RNase solution (10 µL/tube) treatment was performed to remove any RNA contaminant. Further, the solution was incubated at 37ºC for 5 min and proteins were precipitated by adding 200 µL of 6 M NaCl solution. Then, the solution was centrifuged (13000xg, 10 min) at ambient temperature. The supernatant was collected in the microcentrifuge tube and mixed with isopropanol (600 µL/tube). The mixture was placed on ice for 15 min. The same steps were repeated by adding isopropanol and incubated for 20 min. Then, the DNA (precipitate) was carefully cleaned with 70% ethanol (600 µL) and dried at room temperature. The purified DNA was dissolved in 200 µL of buffer (10 mM Tris-HCl, 1 mM EDTA, pH 8.0). Finally, agarose gel electrophoresis was performed to observe isolated DNA.

2.2.8. RNA extraction and cDNA construction

RNA was isolated from untreated cells (control) and Met-AgNPs or Eth-AgNPs treated MCF-7 using the TRIzol method. Briefly, the cell pellet was washed two times with chilled PBS and homogenized in TRIzol reagent followed by the addition of chloroform (200 µL) and then incubated at RT for 15–20 min. The tubes were centrifuged (12000 rpm, 4˚C, 15 min) and the upper aqueous phase was collected into another microcentrifuge tube. The isopropanol (1 mL) was added to the tubes and incubated for 2 hr at -20ºC followed by centrifugation (12000 rpm, 4˚C, 15 min). The precipitate (RNA) was washed two times with 70% ethanol. Then nuclease-free water was added to the pellet and kept at -80ºC for further processing. The Verso cDNA synthesis kit was used for cDNA synthesis from the isolated RNA. A master

mix reaction (20 µl/tube) was prepared using reaction buffer (5x), dNTPs mix (5 mM each), anchored Oligo dT primer (0.5 µg/µL), random hexamer (0.4 µg/µL), verso enzyme mix, and template RNA (1 ng). To verify the formation of the cDNA strand, it was subsequently amplified using Glyceraldehyde 3-phosphate dehydrogenase (GAPDH) housekeeping gene primer pairs. The thermal cycler conditions include initial denaturation (95ºC, 5 min), 35 cycles of denaturation (95ºC,30 sec), annealing (60ºC, 35 sec), and extension (72ºC, 35 sec) followed by a final extension step (72ºC, 7 min). The amplified products were resolved on agarose gel (2%) and synthesized cDNA was stored at -20℃ for further use.

2.2.8.1. Quantitative PCR for mRNA Expression Analysis

The expressions of apoptotic genes (*TP53, CYCS, BCL2L1, BAX*, and *CCND1*) and Caspases (*CASP9*, *CASP8* and *CASP3*) were assessed by using the specific primer pairs (Table 1). A housekeeping gene, *GAPDH*, was used as an internal control. The total reaction volume was made 10 µL by adding 1x SYBR green dye, 10 pM each of forward and reverse primer, and 100 ng/µL cDNA. Thermal cycler conditions comprise a denaturation step (95ºC, 5 min) followed by annealing and extension steps at 53ºC for 30 sec for 40 cycles. The PCR reaction for gene-specific primers and the internal control (*GAPDH)* was carried out in triplicate. To minimize the rate of error, non-template control was also included in each reaction. Finally, the analysis of the melting curve was performed to verify template specificity, and the relative fold change was estimated by the $2^{-\Delta\Delta Ct}$ formula.

Table 1: Primer sequence of genes along with their annealing temperature and amplicon size

Genes	Primer Sequence		Annealing Temp (ºC)	Amplicon Size (bp)
	Forward (5'-3')	Reverse (3'-5')		
TP53	AAGTCTGTGACTTGCACGTACTCC	GTCATGTGCTGTGACTGCTTGTAG	57	152
CYCS	TGGGTGATGTTGAGAAAGGC	ATTGGCGGCTGTGTAAGAG	55	158
BCL2L1	GGTTGACTTTCTCTCCTAC	CGATTCAGTCCCTTCTG	54	103
BAX	GCTGCAGAGGATGATTG	CCTTGAGCACCAGTTTG	53	146
CCND1	CGAAGTGGAAACCATCC	CTCCTTCTGCACACATT	54	130
GAPDH	AGCGAGATCCCTCCAAA	CTTGAGGCTCTTGTCATACT	60	200
CAPS9	GGCTCTTCCTTTGTTCATCTCC	TCACCAAATCCTCCAGAACCA	58	210
CAPS8	GATGTTATTCCAGAGACTCCAG	GGTAGGTAATCAGCAAATCCA	58	110
CASP3	ATGGAAGCGAATCAATGGAC	AAACATCACGCATCAATTCC	57	240

2.2.9. Analysis of MCF-7 cells apoptosis by flow cytometry

MCF-7 cells that were present in the logarithmic growth phase were seeded (1 × 10^6 cells/well) in a 6-well plate and exposed to varying concentrations of Eth-AgNPs and Met-AgNPs (5, 10, and 25 µg/mL). The DMSO (0.01%) treatment was given to control cells as a vehicle control. After 24 hours of incubation,

apoptotic cells induced by Eth-AgNPs and Met-AgNPs were identified with the help of an Annexin V/PI staining kit (BioLegend, USA). In brief, the cells were collected, washed, and mixed with a binding buffer (100 µL) provided with the kit. Then, a mixture (1:1) of Annexin-FITC and PI was added to the tubes. After 30 min, binding buffer (400 µL) was supplemented to the labelled cells. Subsequently, cells were acquired in a Flow Cytometer (Cytomics FC 500; Beckman Coulter, Brea, CA, USA).

2.2.10. Analysis of apoptotic cells morphology

Morphological changes in the MCF-7 cell following treatment with either Met-AgNPs or Eth-AgNPs were directly observed using an inverted fluorescence microscope (Optica, Italy). The cells were placed (0.1 × 10^6 cells/well) into tissue culture plates (6 wells) and allowed to grow overnight in a CO_2 incubator at 37ºC. The next day, the media was discarded and different concentrations of treatment of either Met-AgNPs or Eth-AgNPs were given, and plates were placed in a CO_2 incubator (37ºC, 24 hr). Then, the cells were washed with PBS, and images of each well were captured by inverted fluorescence microscopy.

2.2.11. Analysis RBC haemolysis

The RBC haemolysis test was performed to comprehend the toxicity of the synthesized Met-AgNPs and Eth-AgNPs. The RBC haemolysis test was performed by following the published procedure (Bansal et al. 2015). Briefly, human blood was centrifuged at 2500 rpm for 10 min, and plasma and buffy coat were carefully removed. The RBC cells were washed twice with phosphate-buffered saline. One hundred microliters of 4% RBC cells were taken in microfuge tubes. Then 100 µL of varying concentrations of Met-AgNPs or Eth-AgNPs, such as 200, 100, 50, and 25 µg/mL, were added in respective tubes in triplicate while 100 µL of 1% (v/v) Triton solution and PBS were taken in separate tubes as a positive and negative control, respectively. The reaction tubes were incubated at 37°C for 1 hr. Once the incubation was over, tubes were centrifuged at 2000 rpm for 10 min. Then, 100 µL of supernatants from the tubes were carefully taken and placed in the respective 96 wells in the ELISA plate. The absorbance of the supernatant was measured at 540 nm. The % lysis of RBC was calculated using the following formulas as below:

$$\%\ RBC\ haemolysis = \frac{Absorbance\ of\ sample - Absorbance\ of\ negative\ control}{Absorbance\ of\ positive\ control - Absorbance\ of\ negative\ control}$$

Statistical Analysis

Analysis of variance (ANOVA) test was practiced determining the statistical differences between a pair of data set. The *p-value* < 0.05 was treated as statistically significant between a pair of data sets.

3. Result and discussion

The extraction of phytochemicals/secondary metabolites from the plants/parts of the plant depends on the polarity of solvents and their physiochemical properties (Nawaz et al. 2020). Both methanol and ethanol are polar organic compounds; however, methanol is more polar than ethanol due to the absence of -CH2- electron pumping groups, which reduces the partial negative charge on oxygen molecules. This

decreases the partial charge difference between oxygen and hydrogen in the hydroxyl group of ethanol. Moreover, methanol is among the prominent solvents used to extract phytochemicals from herbs and spices. Ethanol 70% (v/v) contains 30% water molecules, which increase its polarity leading to an increase in the extraction of more polar compounds/hydrophilic secondary metabolite.

Plants contain various secondary metabolites or phytochemicals like carbohydrates, amino acids, proteins, flavonoids, alkaloids, tannins, polyphenols, and saponins (Roy et al. 2019). The differences in solvent polarity, including the addition of 30% water to ethanol (70% v/v), led to varying levels of phytochemical extraction. This, in turn, resulted in differences in the compounds and their quantities, affecting the reduction of Ag^{+} to Ag° and the subsequent stabilization and capping during the synthesis of AgNPs. As a result, AgNPs synthesized from different extracts contain distinct surface functional groups, leading to variations in their antioxidant properties and anticancer efficacy against MCF-7 cells. In contrast to traditional chemical synthesis techniques, this method avoids the toxic compounds usage and high temperatures, providing a secure, and more justifiable alternative. Thus, the current study provides pragmatic evidence that the AgNPs synthesized employing 70% ethanol extract exhibit better anticancer activity against MCF-7 cells as compared to the methanol extract-based AgNPs.

3.1. Silver nanoparticles characterization

3.1.1. UV-Vis Spectroscopy analysis

The mixing of methanolic extract (1 mL) with 10 mM $AgNO_3$ solution (30 mL), causes a gradual colour change from pale yellow to light brown, which was the best primary noticeable index of the formation of AgNPs. Similarly, previous studies observed colour change during the synthesis of AgNPs (Dehghanizade et al. 2018; Masum et al. 2019), which confirmed the completion of the reaction between the phytochemicals present in the methanolic extract and $AgNO_3$ solution. Further, the absorption spectrum of the formed AgNPs (light brown colour) displayed maximum absorption between 300–400 nm, suggesting the reduction of $Ag^{+} \rightarrow Ag^{0}$ in the presence of phytochemical of *Citrus medica* fruit extract and synthesis of AgNPs (Fig. 1A).

Similarly, the absorption spectrum of the synthesized Eth-AgNPs was analyzed and observed absorbance maxima between 320–380 nm (Fig. 1B). The high absorbance between 320–380 nm was due to the surface plasmon phenomenon of the electron cloud present on the surface of AgNPs as evident from the previous observations of ethanolic extract-based synthesis of AgNPs (Mahmoud et al. 2020; Samuggam et al. 2021).

3.1.2. Analysis of AgNPs by FTIR

The Ag ions reduction by the phytocompounds present in the plant extract is attributed to the synthesis of AgNPs; subsequently, these compounds can cause stabilization and capping of AgNPs. The functional groups of these phytocompounds present on the surface of AgNPs were identified by the FTIR

technique. The FTIR spectrum of the Met-AgNPs exhibited major absorption peak shifts at 3468.51, 2927.3, 2854.5, 2090.89, 1749,1634.89 cm^{-1}. Moreover, new absorption peaks appeared at lower wave numbers, such as 1385, 1304, 1250, 1096, 1022, 680, and 456 cm^{-1} (Fig. 2A). The peak shifts as well as the appearance of new peaks, indicate the reducing, stabilizing, and capping actions of the phytocompounds of *C. medica*. A shift in the peak at 3369.32 cm^{-1} to 3468.2 cm^{-1} was due to either O—H or N—H stretching of the phenols available in the plant extract (Bilal et al. 2019). The occurrence of C-H stretching belonging to the aliphatic functional group/methylene group designated by the peak at 2927.3 cm^{-1}. This peak, 2927.3 cm^{-1}, also indicates the existence of triterpenoid saponins (Qais et al. 2019). The peak at 2854.5 cm^{-1} demonstrated the presence of alkenes' asymmetric and symmetric stretches. The absorption peak at 1634.89 cm^{-1} matches the C = C group of aromatic compounds (Raghunandan et al. 2010). The peak at 1385 cm^{-1} signifies the incidence of germinal methyl groups. The peak at 1022 cm^{-1} simplifies the C-O stretching of the ether group (Dehghanizade et al. 2018). On the other hand, the peak at 680 cm^{-1} was owing to the presence of the = CH group of the aromatic compounds.

Likewise Met-AgNPs, the major absorption peaks of the ethanolic extract were observed at 3468.78, 2922, 2852.3, 2087, and 1639.04 cm^{-1} (Fig. 2B). The biosynthesized Eth-AgNPs showed very minor change in the shift of the major spectrum peaks. However, at the lower wave number, the spectrum showed new absorption peaks at 1463.6, 1377.3, 1341, 1320.5, 1120.5, 1100, and 523.25 cm^{-1}. Of these peaks, some of the absorption peaks like 1120.5, 1100, and 523.25 cm^{-1} were absent in the Met-AgNPs spectrum. The result can be concluded that most of the secondary metabolites were common in both extracts; however, some metabolites are different in both extracts.

3.1.3. Size and zeta potential analysis

The mean size and PDI of the Met-AgNPs were observed to be 154.8 nm and 0.206, respectively (Fig. 3A). The small PDI value suggests that the size distribution of the particle was narrowed down, suggesting uniformity of the particles. Similarly, the mean size and PDI of the Eth-AgNPs were measured to be 163 nm and 0.37, respectively (Fig. 3C). The observed ζ-potential of the methanolic and ethanolic extract-based synthesized AgNPs were − 23.6 mV and − 16.75 mV, respectively, advocating the stability of these synthesized AgNPs (Fig. 3B & 3D). The negatively charged functional groups of the various phytocompounds attached to the nanoparticles' surface ascertained the colloidal capability of the prepared AgNPs (Ahn et al. 2019). Further, a graph between particle size and their percent distribution to better comprehend the size distribution was shown (Fig. 3E & F).

The comparative analysis of both Met-AgNPs and Eth-AgNPs suggests that no significant difference in the mean size of AgNPs synthesized from either methanolic extract or 70% ethanolic extract; however, a significant difference in the PDI was observed. The high PDI of Eth-AgNPs might be due inference of ethanol present in the reaction mixture, which was not completely evaporated owing to the synthesis being performed at 70ºC while the boiling point of ethanol is 78ºC. On the contrary, methanol has a

lower boiling point (64ºC). Thus, during the synthesis at 70°C, most of the methanol was evaporated, hence it did not interfere with size measurement. Earlier, Esfanddarani et al. synthesized AgNPs from methanolic extract and 70% ethanolic extract of Malva sylvestris and observed that ethanolic extract-based AgNPs showed smaller particle size distribution as compared to methanolic extract-based AgNPs (Mahmoodi Esfanddarani et al. 2018).

The DLS technique measures the hydrodynamic size of the AgNPs which include an additional hydration layer around the nanoparticles. Hence, the size of the nanoparticles appears larger in comparison to the actual size as determined by the TEM imaging (Zia et al. 2017). Additionally, the hydrodynamic size of AgNPs can also influenced by the adsorption of phytocompounds on the synthesized AgNPs surface. The small variation in the AgNP hydrodynamic size could be due to the attachment of varying amounts of the phytocompounds on the particle's surface (Vanlalveni et al. 2021).

3.1.4. XRD analysis of AgNPs

The crystalline property of the prepared AgNPs was examined by the X-ray diffraction (XRD) analysis. The XRD spectrum of the Met-AgNPs synthesized from the methanolic extract showed prominent six 2θ peaks at 27.8, 38.6, 46.3, 54.8, 64.9, and 77.1° (Fig. 4A). Besides these peaks, some other minor additional peaks were evident, which were due to noise or organic solvent contaminant. These Bragg's diffraction angles correspond to the lattice planes [122], [111], [200], [120], [220], and [311], respectively (Fig. 4A). Ojha et al. have synthesized AgNPs from *Ricinus communis* var. Carmencita leaf extract and XRD diffraction were performed to ascertain the polycrystalline nature of the synthesized AgNPs. They observed diffraction angles at 27.81°, 32.19°, 38.16°, 44.43°, 46.23°, 54.93°, 64.65°, and 77.61°. These diffraction angles correspond to Bragg's diffraction planes [210], [122], [111], [200], [231], [142],[241], [220], and [311], which suggests face-centered cubic structure (Ojha et al. 2017). Thus, the lattice planes of our experimental data suggest that the synthesized Met-AgNPs are polycrystalline in nature, with a face-centered cubic structure.

In contrast, XRD of the Eth-AgNPs showed five 2θ peaks at 27.8°, 32.2°, 46.3°, 57.4°, and 76.6° (Fig. 4B), which corresponds to the Bragg's lattice planes [210], [122], [231], [241], and [311], respectively. Meng et al. have synthesized AgNPs from *Ficus altissima* Blume leaf extract and its polycrystalline nature by performing X-ray diffraction analysis. They observed diffraction angle 2θ values at 27.81°, 32.16°, 38.12°, 44.3°, 46.21°, 54.83°, 57.39°, 64.42° and 77.45°, corresponding to Bragg's diffraction planes [210], [122], [111], [200], [231], [142], [241], [220] and [311] (Meng 2015). Similarly, Hemlata et al., have observed XRD peaks at 32.18°, 38.04°, 46.13°, 54.63° and 77.08° of the AgNPs prepared from *Rininus communis* var. Carmencita leaf extract, which corresponds to the [111], [200], [120], [202], and [311] Bragg's diffraction planes, respectively. Such planes are in agreement with the face-centered cubic structure and polycrystalline nature of the prepared Eth-AgNPs (Hemlata et al. 2020). Thus, the XRD diffraction angle of Eth-AgNPs confirmed the polycrystalline nature with a face-centered cubic structure.

3.1.5. TEM Analysis of AgNPs

HR-TEM pictures were captured at different magnifications for the size and morphology of the AgNPs (Fig. 5). Met-AgNPs TEM images suggest that majorly formed particles were spherical with dimensions of 15–20 nm; however, some particles portray cylindrical morphology (Fig. 5, A-F). Many authors synthesized AgNPs from methanolic extracts of different plants and observed similar sizes and morphologies (Singh and Navneet 2021; Bawazeer et al. 2021). On the other hand, the TEM images of the Eth-AgNPs formed were relatively smaller in size, i.e., ranging from 5–7 nm (Fig. 5, G-L). The ethanolic extract-based AgNPs showed mostly spherical morphology, while a few of them were also observed as cylindrical. Esfanddarani et al. have shown that AgNPs prepared from 70% ethanolic extract showed smaller size and narrow polydispersity index compared to methanolic extract-based AgNPs (Mahmoodi Esfanddarani et al. 2018). At very high magnification (650000X), the fringes were also visible on the particle's surface of both Met-AgNPs and Eth-AgNPs, suggesting a uniform distribution of phytochemical constituents on AgNPs (Fig. 5D).

3.1.5.1. SAED image Analysis of AgNPs

SAED images give crucial information regarding the polycrystalline nature of the synthesized AgNPs (Rani et al. 2020). The result of the SAED image of both Met-AgNPs and Eth-AgNPs showed five bright electron diffraction rings, as seen in Fig. 5F & K, respectively. The presence of a bright ring suggests the pattern of crystal of Ag atom arrangement in the AgNPs. Our obtained data on crystal planes aligns with previous findings (Soshnikova et al. 2018; Yap et al. 2020). The Ag ions reduction in the presence of extracts (methanolic/ethanolic) of Citrus medica fruit led to the corresponding AgNPs synthesis, suggesting the polycrystalline nature of the formed AgNPs, which correlates well with the obtained XRD data. Following our data, an earlier study observed a similar face-centered cubic structure of the prepared AgNPs with five electron diffraction rings, which correspond to the lattice arrangement of [111], [200], [220], [311], and [222] (Kanniah et al. 2023).

3.2. Analysis of Antioxidant Efficacy of AgNPs

The antioxidant action of the extracts (methanolic/ethanolic) and the respective extracts-based AgNPs (Met-AgNPs and Eth-AgNPs) was detected by the DPPH assay. Met-AgNPs exhibited slightly higher scavenging capacity than the Eth-AgNPs (Fig. 6). The methanolic extract alone and Met-AgNPs demonstrated a dose-dependent increase in scavenging activity (Fig. 6A). Similarly, the ethanolic extract alone and its corresponding AgNPs showed comparable free radical scavenging efficacy, also displaying a dose-dependent scavenging effect (Fig. 6B). Moreover, the scavenging efficacy of the methanolic extract and methanolic extract-based AgNPs is significantly higher than ethanolic extract and ethanolic extract-based AgNPs. The IC_{50} values of the free radical inhibition of the Met-AgNPs and Eth-AgNPs were observed to be 424 µg/mL and 382.45 µg/mL, respectively. This finding suggests that methanolic extract and ethanolic extract and their respective AgNPs could not show strong antioxidant activity.

3.3. Analysis of anticancer activity of the AgNPs

Treatment of cancer is still a challenging task for clinicians, especially in the advanced stages. Chemotherapy in the form of monotherapy or combination therapy received some success and prolonged patients' lives to some extent. However, anticancer drugs also cause severe toxicities to healthy cells, leading to deleterious side effects (Ahmad et al. 2021). This limits the patient's survival from a few months to a few years, depending on the age and health. To overcome the toxicity, various strategies have been adopted, and the encapsulation of chemotherapeutics into nanocarriers is a promising approach. However, the approach is complex, expensive, and still causes some form of toxicity to the healthy cells (Ahmad et al. 2021).

The green synthesis of AgNPs was developed, and its potential is being extensively explored by many research groups in the treatment of various cancers. The approach has many attributes that enable it to be a potential candidate for the treatment of cancer (Ratan et al. 2020). Thus, the anticancer efficacy of the developed Met-AgNPs and Eth-AgNPs was analyzed at 24 and 48 hr of incubation on two different human breast cancer cells including MCF-7 and MDA-MB-231 cancer cells. Both formulations, Met-AgNPs and Eth-AgNPs, showed cytotoxic effects in a dose-dependent manner (Fig. 7). At 50 µg/mL dose of Met-AgNPs, nearly 45% growth inhibition was observed at 24 hr of incubation, which was significantly enhanced to 75% when the incubation was extended to 48 hr, suggesting the efficacy of Met-AgNPs against MCF-7 cells (Fig. 7A). As the dose further increased to 100 µg/mL, nearly 72% of the cell death was observed at 24 hr, which increased to 94% with the extension of incubation time to 48 hr (Fig. 7A). Similarly, Met-AgNPs treatment to MDA-MB-231 cells displayed a significant ($p < 0.0001$) reduction in the growth of cancer cells than untreated group (control) with an IC_{50} value of 37.10 µg/mL at 24 hr and 38.91 µg/mL for 48 hr incubation (Fig. 7C). The result indicates that the Met-AgNPs were noticeably effective against both breast cancer cells. Muthukrishnan et al. have shown that methanolic extract-based AgNPs inhibit the growth of Dalton's lymphoma ascites tumor (Muthukrishnan et al. 2018). Additionally, our previous study showed that AgNPs synthesized from the methanolic extract of *Alpinia galanga* exhibit high efficacy against cervical cancer (Ahmad et al. 2024).

To understand whether AgNPs synthesized from extracts in different organic solvents induce varying levels of anticancer activity, and if so, to determine the extent of these differences, we also evaluated the anticancer activity of the AgNPs prepared from ethanolic extract against MCF-7 and MDA-MB-231 cancer cells. The result of the Eth-AgNPs also showed a dose-dependent cell growth inhibition in both cell lines (Fig. 7B, 7D). At 6.25 and 12.5 µg/mL doses, nearly 25% and 53% of the MCF-7 cancer cell growth inhibition was observed, respectively. Further increase of dosage to 25 µg/mL inhibited the growth of almost 87% of cancer cells after 24 hr of incubation, which further enhanced to 90% with the increased incubation time (48 hr). However, further increase of AgNP doses showed no significant inhibition both at 24 and 48 hr of incubation time. The IC_{50} value of the Eth-AgNPs was 11.58 µg/mL, suggesting that Eth-AgNPs are more effective (than Met-AgNPs) in inhibiting the growth of MCF-7 cancer cells. Equivalently, Eth-AgNPs treatment showed a significant ($p < 0.0001$) decrease in the MDA-MB-231 cells viability as compared to untreated group (control) with an IC_{50} value of 29.28 µg/mL and 10.15 µg/mL for 24 hr and 48 hr incubation, respectively (Fig. 7D). The high efficacy of Eth-AgNPs could

be attributed to the additional extraction of hydrophilic secondary metabolites in 70% ethanol, which contains 30% water. Kis et al. synthesized AgNPs from the ethanolic extract of *Populi gammae* and observed significant, dose-dependent growth inhibition in both MCF-7 and lung carcinoma epithelial cell line A549 (Kis et al. 2022). The AgNPs synthesized by aqueous extracts of *L. scindicus* (L-AgNPs) and *P. turgidum* (P-AgNPs_ seeds showed the cytotoxic effect on MDA-MB-231 cells and IC_{50} values were 141.6 µg/mL and 77.59 µg/mL (Alburae et al. 2024). The synthesized AgNPs showed a better cytotoxic effect on MCF-7 cells compared to MDA-MB-231, therefore, further experiments were performed on MCF-7 cells.

3.4. Analysis of Formulation toxicity by RBC haemolysis test

To analyze the toxicity of the synthesized Met-AgNPs and Eth-AgNPs, RBC haemolysis was performed. The results suggest that up to 50 µg/mL of either Met-AgNPs or Eth-AgNPs caused < 1% of RBC haemolysis. The concentration of AgNPs further increased to 100 µg/mL; the lysis was slightly increased in both extract-based AgNPs. However, further increase of AgNPs concentration to 200 µg/mL, the RBC lysis is significantly increased in both AgNPs, especially more prominently increased in Eth-AgNPs. Importantly, our in-house formulations, Met-AgNPs, and Eth-AgNPs showed high toxicity to the cancer cells (MCF-7) at 100 µg/mL. However, this concentration causes little haemolysis to the RBC cells (< 2%). It was reported that < 5% RBC haemolysis of the formulation is safe for in vivo study.

3.5. Analysis of the molecular mechanism

3.5.1. DNA fragment analysis

DNA fragmentation is one of the peculiar features of apoptosis (Alharbi and Alsubhi, 2022). DNA fragment analysis revealed a thinner band in samples treated with Met-AgNPs or Eth-AgNPs compared to the control, indicating smaller DNA fragments. *This was particularly evident in the smear in Eth-AgNP-treated cells. However, no clear smear in Met-AgNPs treated samples (lane 3) was evident owing to relatively less fragmentation.* This suggests that Eth-AgNPs were more effective in breaking intact DNA, corroborating the MTT assay of Eth-AgNPs treated MCF-7 cells. A similar observation has been reported in A549 cells treated with AgNPs prepared from *Azadirachta indica* (Alharbi and Alsubhi 2022).

3.5.2. Analysis of the molecular mechanism of apoptosis

To unravel the molecular mechanism behind the induction of apoptosis of the MCF-7 cells treated with either Met-AgNPs or Eth-AgNPs, the expression of some of the genes involved in the intrinsic pathways, *viz.*, CCND1 (Cyclin D1) and CYCS (Cytochrome C) (Fig. 10A). The earlier gene implies the progression of the cell cycle's G1 phase to the S phase, while the later gene is a small haem regulating protein of the mitochondria. Also, the extrinsic pathways, *viz.*, proapoptotic *TP53, BAX*, and antiapoptotic *BCL2L1* were analyzed by using their respective primer listed in Table 1. Earlier studies suggest that the AgNPs

promote tumor cell death primarily through apoptosis, which is mediated by the activation of the Bcl-2 protein family, encompassing both proapoptotic and antiapoptotic proteins that regulate cellular sensitivity at the mitochondrial level. Similarly, the key members of the Bcl-2 family play a crucial role in how tumor cells respond to the various AgNPs formulations by which they are treated. For instance, Bax, a proapoptotic protein target, p53, can trigger apoptosis in cancer cells, while BCL2LI, an antiapoptotic protein, can inhibit both autophagy and apoptosis, contributing to cancer cell survival (Bao et al. 2022).

The mRNA expression of the proapoptotic *BAX* gene either treated with Met-AgNPs or Eth-AgNPs displayed significantly increased expression as compared to control ($p < 0.05$). However, the antiapoptotic *BCL2L1* gene mRNA expression of the MCF-7 cells either treated with Met-AgNPs or Eth-AgNPs showed downregulation as compared to the control. *TP53*, another tumor suppressor gene is essential for regulating cell cycle arrest, senescence, and apoptosis, helping to eliminate severely damaged cells. It directly impacts the intrinsic apoptosis pathway by controlling mitochondrial outer membrane permeabilization. It is activated through specific posttranslational modifications, and majorly determines the cell's fate such as, whether to repair DNA, halt the cell cycle, undergo apoptosis, or enter senescence (Yuan et al. 2018). Similarly, our results suggest that the Met-AgNPs showed relatively higher expression of tumor suppressor *TP53* gene as compared to Eth-AgNPs treated MCF-7 cancer cells. *Cyclin D1*, an antiapoptotic gene as well as an important regulator of the cell cycle is involved in promoting cancer by leading to uncontrolled cell growth. In normal cells, the expression of *Cyclin D1* is controlled, but in cancer cells, there is often an increase in the activity of *Cyclin D1* due to different mechanisms (Montalto and De Amicis 2020). Similarly, our result also showed overexpression of mRNA of the *CCND1* gene treated with either Met-AgNPs or Eth-AgNPs as compared to control which aligns with the previously established literature (Bao et al. 2022).

Another crucial gene in the process of apoptosis is cytochrome c. It plays a pivotal role in the functioning of mitochondria and is essential for the intrinsic pathway of apoptosis. Cancer cells often impede the release of cytochrome c from the mitochondria, allowing them to evade programmed cell death (PCD). This ability to avoid apoptosis supports the growth and survival of tumors (Pessoa 2022). In the present study, it was found that the *CYCS* gene was overexpressed when treated with either Met-AgNPs or Eth-AgNPs when compared with the control. However, it was observed that the expression of the *CCND1* gene in both Met-AgNPs and Eth-AgNPs was not statistically significant. Thus, the above findings suggest that the synthesized Met-AgNPs or Eth-AgNPs induce the upregulation of proapoptotic *TP53* and *BAX* genes, an extrinsic pathway, that promotes PCD of MCF-7 cancer cells.

Yuan et al. have treated human cervical cancer with AgNPs synthesized from sinigrin, a reducing and stabilizing agent, and observed upregulation of *TP53, CYCS, BAX*, and *BAK1* genes, suggesting that the synthesized AgNPs induced apoptosis leading to higher inhibition of cancer cells growth (Yuan et al. 2018). Our result suggests that the synthesized Met-AgNPs or Eth-AgNPs besides inducing intrinsic pathways, can also activate extrinsic pathways to promote apoptosis in MCF-7 cancer cell lines. *BAX* and *CYCS* gene expression were statistically significant in AgNP-treated groups, while *TP53* and *BCL2L1* gene expression showed no significant difference. Our data does not distinctly differentiate gene

expression levels between the AgNP-treated groups. However, it indicates that the synthesized AgNPs were highly effective in inducing both extrinsic and intrinsic apoptosis pathways, significantly killing MCF-7 cancer cells, as confirmed by the above cytotoxic assay (Fig. 7). To strengthen the findings of apoptotic and anti-apoptotic gene expressions, we evaluated the CASP3, CASP8, and CASP9 mRNA expression in MCF-7 cells (Fig. 10B). We observed that cells treated with Met-AgNPs or Eth-AgNPs showed comparatively higher expression of CASP3 (executor caspase) compared to CASP8 and CASP9. Our results suggest that slightly higher expression of CASP3 of Eth-AgNPs treated cells is supported by higher expression of TP53, CYCS, and BAX, which are important downstream molecules that initiate the mitochondrial apoptotic pathway (Ullah et al., 2020). Thus, the findings correlate that the activated molecules induce apoptosis, leading to cell death. The observed increase mRNA expression of CASP3 implies that Eth-AgNPs significantly activates the transcriptional machinery involved in apoptosis. Moreover, CASP8 expression in Eth-AgNPs treated cells are notably higher. Thus, the findings suggest that Eth-AgNPs induces apoptosis through the intrinsic mitochondrial pathway, which is described by increased expression of P53, BAX, CYCS, and downstream molecule CASP3 (Baharar et al., 2015). In succinct, the AgNPs synthesized from ethanolic extract promote apoptosis in MCF-7 cells, whereas Met-AgNPs had less effect on these apoptotic genes.

Figure 10A. Relative mRNA expression of genes of MCF-7 cancer cell lines treated with either Met-AgNPs or Eth-AgNPs. (A) *TP53* gene expression, *p*-value between Untreated *vs.* Meth-AgNPs < 0.05; (B) *CCDN1* gene expression, *p*-value Untreated *vs.* Meth-AgNPs < 0.05; Untreated *vs.* Eth-AgNPs < 0.05. (C) *CYCS* gene expression, *p*-value Untreated *vs.* Meth-AgNPs < 0.05, Untreated *vs.* Eth-AgNPs < 0.05. (D). (E) *BAX* gene expression, *p*-value between Untreated *vs.* Met-AgNPs < 0.05 and Untreated *vs.* Eth-AgNPs < 0.05. (E) *BCL2L1* gene expression, *p*-values Untreated *vs.* Meth-AgNPs < 0.05, Untreated *vs.* Eth-AgNPs < 0.05.

3.5.3. Flow cytometry Analysis of Apoptosis

The process of apoptosis plays a pivotal role in the homeostasis of cells. Many morphological and biochemical changes enable us to characterize this phenomenon. The biosynthesized Met-AgNPs and Eth-AgNPs induce apoptosis in MCF-7 cell death in a concentration-dependent manner. Thus, Annexin V/PI was utilized to comprehend the MCF-7 cell death mechanism, viz., apoptosis or non-apoptosis. The result suggests that Met-AgNPs treated cells didn't show a dose-dependent increase of cells in the late stage of apoptosis; however, an increased number of cells were observed in the initial phase of apoptosis from 5 µg/mL to 25 µg/mL of treated dose. On the other hand, at similar doses, Eth-AgNPs showed a consistent increase in the number of cells to the early stage of apoptosis; however, at 25 µg/mL of dose, a significant increase of late stage of MCF-7 cell apoptosis (8.14%) (Fig. 11). This result is in concordance with the cell proliferation assay.

3.4.3.1. Analysis of morphological change

The morphological changes of the MCF-7 cells treated with different doses, either Met-AgNPs or Eth-AgNPs, were analyzed by inverted fluorescence microscopy. The treatment with 5, 10, and 25 µg/mL

doses of Met-AgNPs to MCF-7 cells showed a dose-dependent morphological change, highlighted with red circles (Fig. 12). On the other hand, MCF-7 cells treated with Eth-AgNPs showed notable changes in the morphology in a concentration-dependent manner. At 5 µg/mL, very few cells showed morphological changes, while at 10 µg/mL, a remarkable number of cells exhibit morphological changes, and only a few cells are visible in a normal morphology. However, at 25 µg/mL of dose, almost all cells showed morphological changes. The result is in concordance with the cell proliferation assay.

4. Conclusion

The organic extracts of nutraceutical *Citrus medica* fruits viz. methanolic and ethanolic-based AgNPs were synthesized to evaluate the influence of different organic solvent extracts in the physiochemical characteristics of the particles and their anticancer efficacy against breast cancer cells. The functional metabolites of the *Citrus medica* fruit were involved in the formation of both AgNPs and have a polycrystalline nature. In addition, the size of Eth-AgNPs was smaller than Met-AgNPs. The Eth-AgNPs showed high efficacy in inducing apoptosis in MCF-7 cancer cell lines compared to Met-AgNPs. Eth-AgNPs showed extensive DNA fragmentation as compared to Met-AgNPs treated cells. The proapoptotic genes (*TP53* and *BAX*) showed upregulation while the antiapoptotic gene (*BCL1L2*) showed downregulation, suggesting that either Eth-AgNPs or Met-AgNPs activate extrinsic pathway to induce apoptosis in the MCF-7 treated cancer cells. Moreover, these AgNPs also induce upregulation of mRNA expression of *CCND1* and *CYCS* genes. Thus, besides inducing extrinsic pathways, these AgNPs can activate the intrinsic pathway of apoptosis. Further, Eth-AgNPs treatment induces extensive apoptosis in MCF-7 cells, which was further corroborated by morphological analysis. Therefore, the synthesized AgNPs were effective in killing MCF-7 cancer cells. In succinct, ethanolic extract-based AgNPs are more effective in inducing apoptosis, which led to high efficacy in inhibiting/killing MCF-7 breast cancer cells. Thus, we can conclude that preparing AgNPs from the organic extract of either methanol or ethanol to evaluate their anticancer efficacy. The addition of water in the ethanol would be proven to generate effective AgNPs to kill/inhibit the higher number of MCF-7 cells compared to methanolic extract-based AgNPs. Future studies are warranted to decipher the role of effective plant metabolite extraction methods to generate more efficient anticancer AgNP-based therapeutics for tumors.

Limitation of the study: The plant extract containing phytocompounds are better reducing and stabilizing agents for the synthesis of AgNPs compared to the chemically synthesized AgNPs (Nie et al. 2024). However, several factors including pH, temperature, choice of reductant, capping agents, zeta potential etc. determined the stability of AgNPs. Therefore, a comprehensive stability assessment is required for the synthesized AgNPs (Met-AgNPs and Eth-AgNPs). Further, the toxicity of AgNPs was attributed to its size, concentration, shape, surface charge, and surface chemistry. Therefore, the synthesized AgNPs (Met-AgNPs and Eth-AgNPs) need to be inspected *in-vivo* conditions for their toxicity in biological environments.

Abbreviations

Silver nanoparticles (AgNPs), Methanolic extract-based AgNPs (Met-AgNPs), Ethanolic extract-based AgNPs (Eth-AgNPs), Fourier Transform Infrared (FTIR), High-Resolution Transmission Electron Microscopy (HR-TEM), Selected Area Electron Diffraction (SAED), X-Ray Diffraction (XRD), Michigan Cancer Foundation (MCF-7), Sulforhodamine B (SRB), Glyceraldehyde 3-phosphate dehydrogenase (GAPDH), Dimethyl sulfoxide (DMSO), Polydispersity Index (PDI), Cytochrome C (CYCS), Cyclin D1 (CCND1), Programmed cell death (PCD)

Declarations

Availability of data and materials: Not applicable

Competing interest: The authors affirm no competing interests.

Funding: We are grateful to the Department of Biotechnology, Ministry of Science and Technology, India for providing financial support under the Grant ID: BT/INF/22/SP33063/2019.

Authors contributions

Conceptualization: Ejaj Ahmad, Sundeep Singh Saluja; **Methodology**: Ejaj Ahmad, Mohammed Sajid, Alina Athar, Arun Kumar, and Mohammad Zulfazal Ahmed; **Formal Analysis and Investigation**: Ejaj Ahmad, Alina Athar, Mohammed Sajid, Arun Kumar, Abhay Kumar Sharma, Mohammad Zulfazal Ahmed, and Nimisha; **Original draft**: Ejaj Ahmad, Alina Athar and Mohammed Sajid; **Revise the draft critically:** Ejaj Ahmad, Mohammed Sajid, Mausumi Bharadwaj, **Ali Saeed Alqahtani**; **Funding acquisition, Resources and supervision**: Sundeep Singh Saluja. All authors read and approved the final manuscript.

Acknowledgment: Govind Ballabh Pant Institute of Postgraduate Medical Education and Research, New Delhi, India, is admired for the facilities provided for this study. This work was supported by the Department of Biotechnology, Ministry of Science and Technology, Government of India with grant no. BT/INF/22/SP33063/2019.

References

1. Ahmad E, Ali A, Fatima MT, et al (2021) Ligand decorated biodegradable nanomedicine in the treatment of cancer. Pharmacol Res 167:105544. https://doi.org/10.1016/j.phrs.2021.105544
2. Ahmad E, Athar A, Nimisha, et al (2024) Harnessing nature's potential: Alpinia galanga methanolic extract mediated green synthesis of silver nanoparticle, characterization and evaluation of anti-neoplastic activity. Bioprocess Biosyst Eng 47:1183–1196. https://doi.org/10.1007/s00449-024-02993-7
3. Ahn E-Y, Jin H, Park Y (2019) Assessing the antioxidant, cytotoxic, apoptotic and wound healing properties of silver nanoparticles green-synthesized by plant extracts. Mater Sci Eng C Mater Biol

Appl 101:204–216. https://doi.org/10.1016/j.msec.2019.03.095

4. Alburae, N., Alshamrani, R. & Mohammed, A.E. Bioactive silver nanoparticles fabricated using *Lasiurus scindicus* and *Panicum turgidum* seed extracts: anticancer and antibacterial efficiency. Sci Rep 14, 4162 (2024). https://doi.org/10.1038/s41598-024-54449-3
5. Alharbi NS, Alsubhi NS (2022) Green synthesis and anticancer activity of silver nanoparticles prepared using fruit extract of Azadirachta indica. Journal of Radiation Research and Applied Sciences 15:335–345. https://doi.org/10.1016/j.jrras.2022.08.009
6. Antropova IG, Revina AA, Oo PM, et al (2021) Synthesis of Silver Nanoparticles Using Reactive Water-Ethanol Extracts from Murraya paniculata. ACS Omega 6:8313–8321. https://doi.org/10.1021/acsomega.1c00019
7. Bansal R, Pathak R, Jha D, et al (2015) Enhanced Antimicrobial Activity of Amine-Phosphonium (N-P) Hybrid Polymers Against Gram-Negative and Gram-Positive Bacteria. International Journal of Polymeric Materials and Polymeric Biomaterials 64:84–89. https://doi.org/10.1080/00914037.2014.886246
8. Bao J, Jiang Z, Ding W, et al (2022) Silver nanoparticles induce mitochondria-dependent apoptosis and late non-canonical autophagy in HT-29 colon cancer cells. Nanotechnol Rev 11:1911–1926. https://doi.org/10.1515/ntrev-2022-0114
9. Bawazeer S, Rauf A, Shah SUA, et al (2021) Green synthesis of silver nanoparticles using *Tropaeolum majus*: Phytochemical screening and antibacterial studies. Green Processing and Synthesis 10:85–94. https://doi.org/10.1515/gps-2021-0003
10. Benedetto N, Carlucci V, Faraone I, et al (2023) An Insight into Citrus medica Linn.: A Systematic Review on Phytochemical Profile and Biological Activities. Plants 12:. https://doi.org/10.3390/plants12122267
11. Bhakya S, Muthukrishnan S, Sukumaran M, Muthukumar M (2016) Biogenic synthesis of silver nanoparticles and their antioxidant and antibacterial activity. Appl Nanosci 6:755–766. https://doi.org/10.1007/s13204-015-0473-z
12. Bitwell C, Indra SS, Luke C, Kakoma MK (2023) A review of modern and conventional extraction techniques and their applications for extracting phytochemicals from plants. Scientific African 19:e01585. https://doi.org/10.1016/j.sciaf.2023.e01585
13. Bray F, Laversanne M, Sung H, et al (2024) Global cancer statistics 2022: GLOBOCAN estimates of incidence and mortality worldwide for 36 cancers in 185 countries. CA Cancer J Clin 74:229–263. https://doi.org/10.3322/caac.21834
14. Chitsazi MR, Korbekandi H, Asghari G, et al (2016) Synthesis of silver nanoparticles using methanol and dichloromethane extracts of Pulicaria gnaphalodes (Vent.) Boiss. aerial parts. Artif Cells Nanomed Biotechnol 44:328–333. https://doi.org/10.3109/21691401.2014.949726
15. Chouhan N (2018) Silver nanoparticles: synthesis, characterization and applications. In: Maaz K (ed) Silver Nanoparticles - Fabrication, Characterization and Applications. InTech

16. Das S, Das J, Samadder A, et al (2013) Biosynthesized silver nanoparticles by ethanolic extracts of Phytolacca decandra, Gelsemium sempervirens, Hydrastis canadensis and Thuja occidentalis induce differential cytotoxicity through G2/M arrest in A375 cells. Colloids Surf B Biointerfaces 101:325–336. https://doi.org/10.1016/j.colsurfb.2012.07.008
17. Davidson A (2006) The oxford companion to food. Oxford University Press
18. Dehghanizade S, Arasteh J, Mirzaie A (2018) Green synthesis of silver nanoparticles using Anthemis atropatana extract: characterization and in vitro biological activities. Artif Cells Nanomed Biotechnol 46:160–168. https://doi.org/10.1080/21691401.2017.1304402
19. Heidari Z, Salehzadeh A, Sadat Shandiz SA, Tajdoost S (2018) Anti-cancer and anti-oxidant properties of ethanolic leaf extract of Thymus vulgaris and its bio-functionalized silver nanoparticles. 3 Biotech 8:177. https://doi.org/10.1007/s13205-018-1199-x
20. Hemlata, Meena PR, Singh AP, Tejavath KK (2020) Biosynthesis of Silver Nanoparticles Using Cucumis prophetarum Aqueous Leaf Extract and Their Antibacterial and Antiproliferative Activity Against Cancer Cell Lines. ACS Omega 5:5520–5528. https://doi.org/10.1021/acsomega.0c00155
21. Jain N, Jain P, Rajput D, Patil UK (2021) Green synthesized plant-based silver nanoparticles: therapeutic prospective for anticancer and antiviral activity. Micro and Nano Syst Lett 9:5. https://doi.org/10.1186/s40486-021-00131-6
22. Jiang Y, Jiang Z, Wang M, Ma L (2022) Current understandings and clinical translation of nanomedicines for breast cancer therapy. Adv Drug Deliv Rev 180:114034. https://doi.org/10.1016/j.addr.2021.114034
23. Kanniah P, Balakrishnan S, Subramanian ER, et al (2023) Preliminary investigation on the impact of engineered PVP-capped and uncapped silver nanoparticles on Eudrilus eugeniae, a terrestrial ecosystem model. Environ Sci Pollut Res Int 30:25239–25255. https://doi.org/10.1007/s11356-022-21898-0
24. Khan ZUH, Khan A, Chen Y, et al (2017) Biomedical applications of green synthesized Nobel metal nanoparticles. J Photochem Photobiol B, Biol 173:150–164. https://doi.org/10.1016/j.jphotobiol.2017.05.034
25. Kharissova OV, Kharisov BI, Oliva González CM, et al (2019) Greener synthesis of chemical compounds and materials. R Soc Open Sci 6:191378. https://doi.org/10.1098/rsos.191378
26. Kis B, Moacă E-A, Tudoran LB, et al (2022) Green Synthesis of Silver Nanoparticles Using Populi gemmae Extract: Preparation, Physicochemical Characterization, Antimicrobial Potential and In Vitro Antiproliferative Assessment. Materials (Basel) 15:. https://doi.org/10.3390/ma15145006
27. Mahmoodi Esfanddarani H, Abbasi Kajani A, Bordbar A-K (2018) Green synthesis of silver nanoparticles using flower extract of Malva sylvestris and investigation of their antibacterial activity. IET Nanobiotechnol 12:412–416. https://doi.org/10.1049/iet-nbt.2017.0166
28. Mahmoud A, Mohamed B, Ibraheem I, et al (2020) [PDF] Characterization of Ulva fasciata Ethanolic Extract-mediated Biosynthesized Silver Nanoparticles and Evaluation of their Nephrocadiopreventive

Effects in Doxorubicin-injected Wistar Rats | Semantic Scholar. Advances in Animal and Veterinary Sciences

29. Masum MMI, Siddiqa MM, Ali KA, et al (2019) Biogenic Synthesis of Silver Nanoparticles Using Phyllanthus emblica Fruit Extract and Its Inhibitory Action Against the Pathogen Acidovorax oryzae Strain RS-2 of Rice Bacterial Brown Stripe. Front Microbiol 10:820. https://doi.org/10.3389/fmicb.2019.00820
30. Meng Y (2015) A sustainable approach to fabricating ag nanoparticles/pva hybrid nanofiber and its catalytic activity. Nanomaterials (Basel) 5:1124–1135. https://doi.org/10.3390/nano5021124
31. Muthukrishnan S, Vellingiri B, Murugesan G (2018) Anticancer effects of silver nanoparticles encapsulated by Gloriosa superba (L.) leaf extracts in DLA tumor cells. Future Journal of Pharmaceutical Sciences 4:206–214. https://doi.org/10.1016/j.fjps.2018.06.001
32. Nahvi I, Belkahla S, Biswas S, Chakraborty S (2022) A review on nanocarrier mediated treatment and management of triple negative breast cancer: A saudi arabian scenario. Front Oncol 12:953865. https://doi.org/10.3389/fonc.2022.953865
33. Nawaz H, Shad MA, Rehman N, et al (2020) Effect of solvent polarity on extraction yield and antioxidant properties of phytochemicals from bean (Phaseolus vulgaris) seeds. Braz J Pharm Sci 56:. https://doi.org/10.1590/s2175-97902019000417129
34. Nie P, Zhao Y, Xu H. Synthesis, applications, toxicity and toxicity mechanisms of silver nanoparticles: A review. Ecotoxicol Environ Saf. 2023 Mar 15;253:114636. https://doi.org/10.1016/j.ecoenv.2023.114636.
35. Odularu AT (2018) Metal nanoparticles: thermal decomposition, biomedicinal applications to cancer treatment, and future perspectives. Bioinorg Chem Appl 2018:9354708. https://doi.org/10.1155/2018/9354708
36. Ojha S, Sett A, Bora U (2017) Green synthesis of silver nanoparticles by*Ricinus communis* var.*carmencita* leaf extract and its antibacterial study. Adv Nat Sci: Nanosci Nanotechnol 8:035009. https://doi.org/10.1088/2043-6254/aa724b
37. Pessoa J (2022) Cytochrome c in cancer therapy and prognosis. Biosci Rep 42:. https://doi.org/10.1042/BSR20222171
38. Qais FA, Shafiq A, Khan HM, et al (2019) Antibacterial Effect of Silver Nanoparticles Synthesized Using Murraya koenigii (L.) against Multidrug-Resistant Pathogens. Bioinorg Chem Appl 2019:4649506. https://doi.org/10.1155/2019/4649506
39. Raghunandan D, Bedre MD, Basavaraja S, et al (2010) Rapid biosynthesis of irregular shaped gold nanoparticles from macerated aqueous extracellular dried clove buds (Syzygium aromaticum) solution. Colloids Surf B Biointerfaces 79:235–240. https://doi.org/10.1016/j.colsurfb.2010.04.003
40. Rahman M, Afzal O, Ullah SNMN, et al (2023) Nanomedicine-Based Drug-Targeting in Breast Cancer: Pharmacokinetics, Clinical Progress, and Challenges. ACS Omega 8:48625–48649. https://doi.org/10.1021/acsomega.3c07345

41. Ratan ZA, Haidere MF, Nurunnabi M, et al (2020) Green chemistry synthesis of silver nanoparticles and their potential anticancer effects. Cancers (Basel) 12:. https://doi.org/10.3390/cancers12040855
42. Roy A, Bulut O, Some S, et al (2019) Green synthesis of silver nanoparticles: biomolecule-nanoparticle organizations targeting antimicrobial activity. RSC Adv 9:2673–2702. https://doi.org/10.1039/C8RA08982E
43. Samuggam S, Chinni SV, Mutusamy P, et al (2021) Green Synthesis and Characterization of Silver Nanoparticles Using Spondias mombin Extract and Their Antimicrobial Activity against Biofilm-Producing Bacteria. Molecules 26:. https://doi.org/10.3390/molecules26092681
44. Sharma A, Goyal AK, Rath G (2018) Recent advances in metal nanoparticles in cancer therapy. J Drug Target 26:617–632. https://doi.org/10.1080/1061186X.2017.1400553
45. Sharma VK, Yngard RA, Lin Y (2009) Silver nanoparticles: green synthesis and their antimicrobial activities. Adv Colloid Interface Sci 145:83–96. https://doi.org/10.1016/j.cis.2008.09.002
46. Singh R, Navneet (2021) Green synthesis of silver nanoparticles using methanol extract of Ipomoea carnea Jacq. to combat multidrug resistance bacterial pathogens. Current Research in Green and Sustainable Chemistry 4:100152. https://doi.org/10.1016/j.crgsc.2021.100152
47. Soshnikova V, Kim YJ, Singh P, et al (2018) Cardamom fruits as a green resource for facile synthesis of gold and silver nanoparticles and their biological applications. Artif Cells Nanomed Biotechnol 46:108–117. https://doi.org/10.1080/21691401.2017.1296849
48. Sung H, Ferlay J, Siegel RL, et al (2021) Global cancer statistics 2020: GLOBOCAN estimates of incidence and mortality worldwide for 36 cancers in 185 countries. CA Cancer J Clin 71:209–249. https://doi.org/10.3322/caac.21660
49. Tagde P, Najda A, Nagpal K, et al (2022) Nanomedicine-Based Delivery Strategies for Breast Cancer Treatment and Management. Int J Mol Sci 23:. https://doi.org/10.3390/ijms23052856
50. Vanlalveni C, Lallianrawna S, Biswas A, et al (2021) Green synthesis of silver nanoparticles using plant extracts and their antimicrobial activities: a review of recent literature. RSC Adv 11:2804–2837. https://doi.org/10.1039/d0ra09941d
51. Vichai V, Kirtikara K (2006) Sulforhodamine B colorimetric assay for cytotoxicity screening. Nat Protoc 1:1112–1116. https://doi.org/10.1038/nprot.2006.179
52. Wu D, Si M, Xue H-Y, Wong H-L (2017) Nanomedicine applications in the treatment of breast cancer: current state of the art. Int J Nanomedicine 12:5879–5892. https://doi.org/10.2147/IJN.S123437
53. Yap YH, Azmi AA, Mohd NK, et al (2020) Green synthesis of silver nanoparticle using water extract of onion peel and application in the acetylation reaction. Arab J Sci Eng 45:4797–4807. https://doi.org/10.1007/s13369-020-04595-3
54. Yuan Y-G, Zhang S, Hwang J-Y, Kong I-K (2018) Silver nanoparticles potentiates cytotoxicity and apoptotic potential of camptothecin in human cervical cancer cells. Oxid Med Cell Longev 2018:6121328. https://doi.org/10.1155/2018/6121328

55. Ullah I, Khalil AT, Ali M, Iqbal J, Ali W, Alarifi S, Shinwari ZK (2020) Green-Synthesized Silver Nanoparticles Induced Apoptotic Cell Death in MCF-7 Breast Cancer Cells by Generating Reactive Oxygen Species and Activating Caspase 3 and 9 Enzyme Activities. Oxid Med Cell Longev. 2020:1215395.
56. Baharara J, Namvar F, Ramezani T, Mousavi M, Mohamad R (2015) Silver nanoparticles biosynthesized using Achillea biebersteinii flower extract: apoptosis induction in MCF-7 cells via caspase activation and regulation of Bax and Bcl-2 gene expression. Molecules 2015: 20(2):2693-706.
57. Zhang X-F, Liu Z-G, Shen W, Gurunathan S (2016) Silver nanoparticles: synthesis, characterization, properties, applications, and therapeutic approaches. Int J Mol Sci 17:. https://doi.org/10.3390/ijms17091534
58. Zia Q, Mohammad O, Rauf MA, et al (2017) Biomimetically engineered Amphotericin B nano-aggregates circumvent toxicity constraints and treat systemic fungal infection in experimental animals. Sci Rep 7:11873. https://doi.org/10.1038/s41598-017-11847-0
59. Zuhrotun A, Oktaviani DJ, Hasanah AN (2023) Biosynthesis of gold and silver nanoparticles using phytochemical compounds. Molecules 28:. https://doi.org/10.3390/molecules28073240

Figures

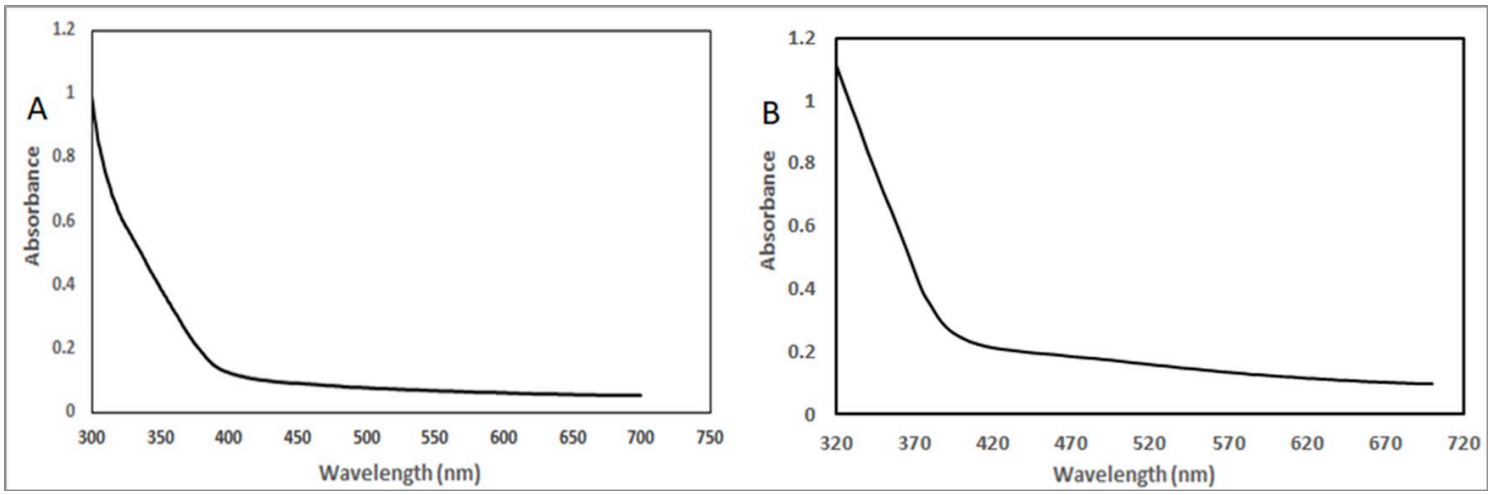

Figure 1

UV-visible spectrum of the AgNPs synthesized from *Citrus medica* fruit extract. (A) Met-AgNPs; (B) Eth-AgNPs.

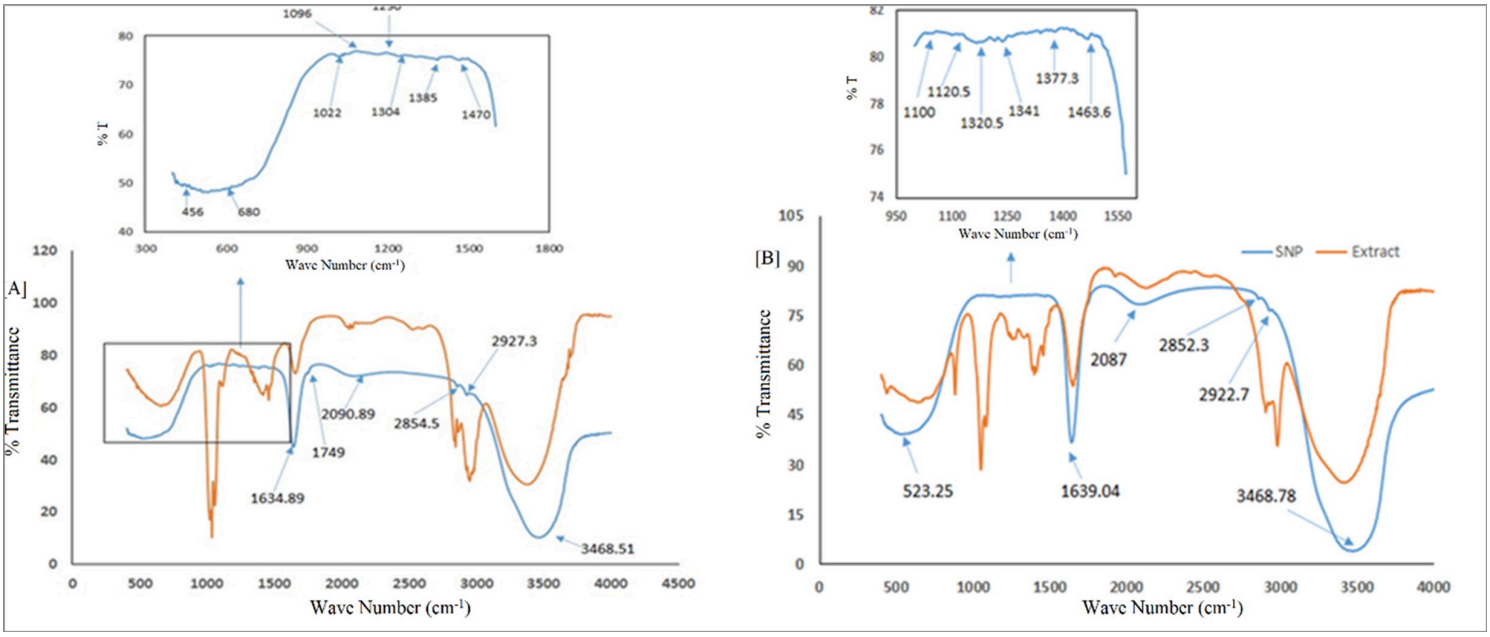

Figure 2

FTIR spectrum of biosynthesized AgNPs. (A) Methanolic extract and Met-AgNPs; (B) ethanolic extract and Eth-AgNPs.

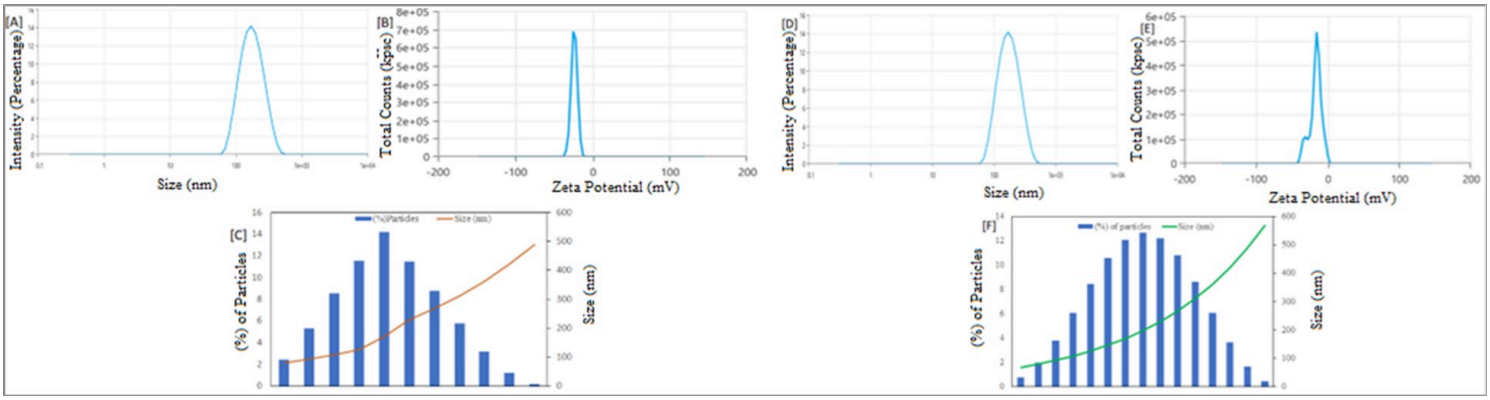

Figure 3

AgNPs size analysis using DLS. Methanolic extract-based biosynthesized AgNPs; (A) Mean size (B) ζ-Potential and (E) Size *vs.* percentage of Met-AgNPs. Ethanolic extract-based biosynthesized AgNPs; (C) Mean size, (D) ζ-Potential, and (F) Size *vs.* percentage of synthesized Eth-AgNPs.

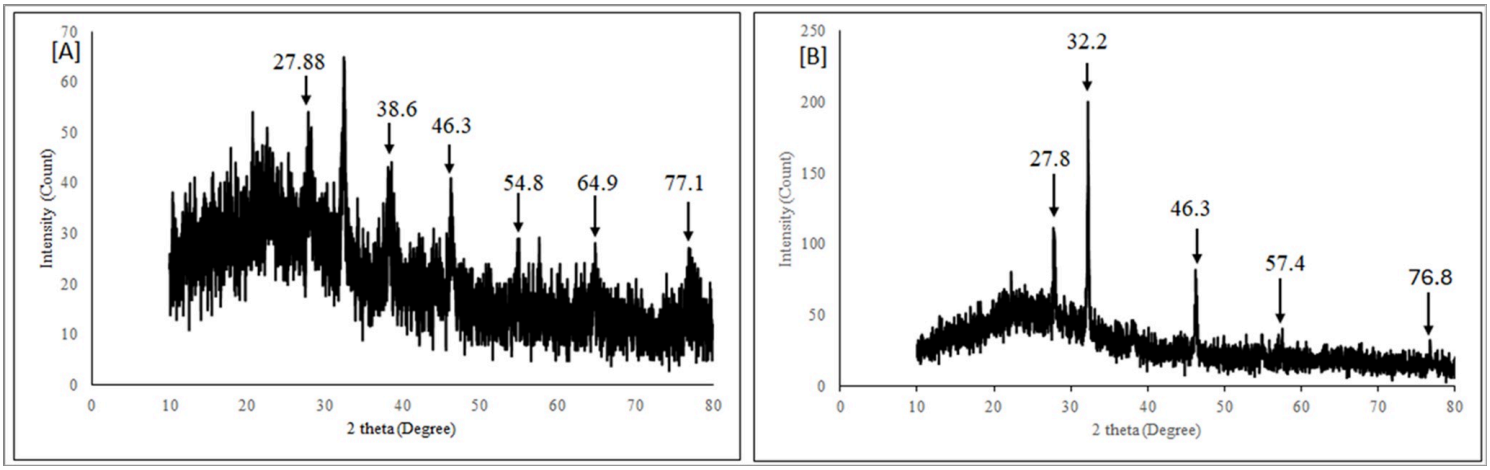

Figure 4

XRD spectrum of the biosynthesized AgNPs. (A) Met-AgNPs; (B) Eth-AgNPs.

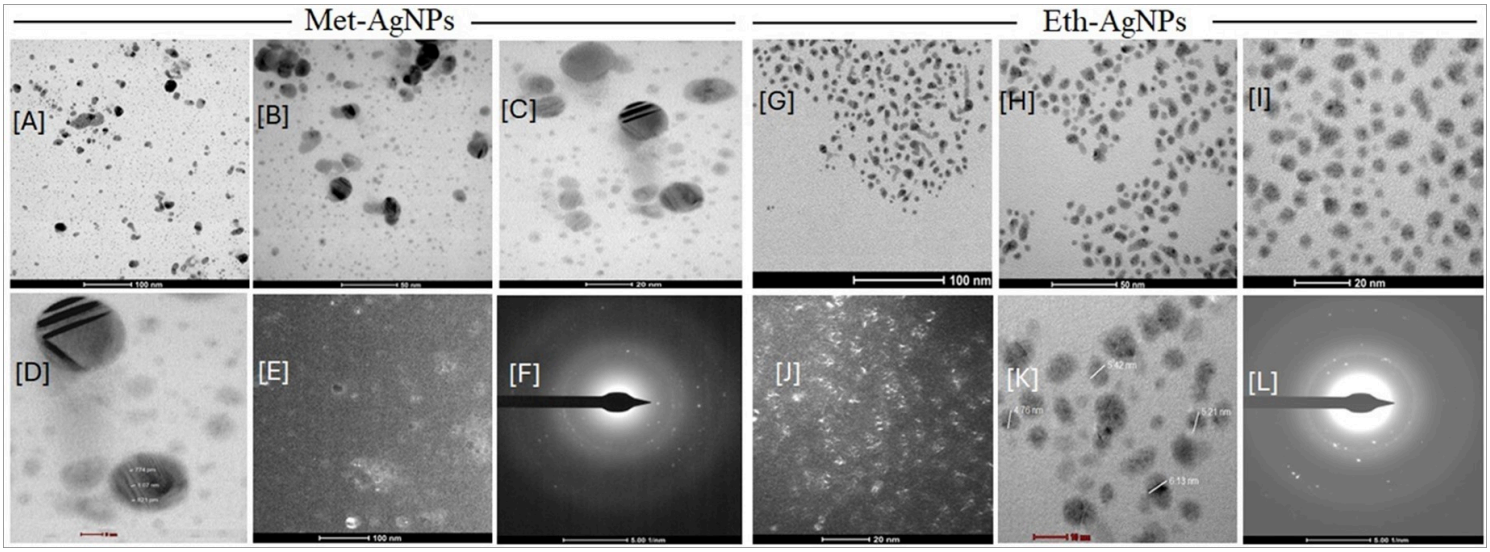

Figure 5

TEM images of Met-AgNPs (A-F) with varying magnifications (A-C); Dark Field image (D) HR-TEM image with fringes (E) and SAED image of AgNPs (F). TEM images of Eth-AgNPs (G-L) with varying magnifications (G-I); Dark Field image (J) HR-TEM image with fringes (K) and SAED image of AgNPs (L).

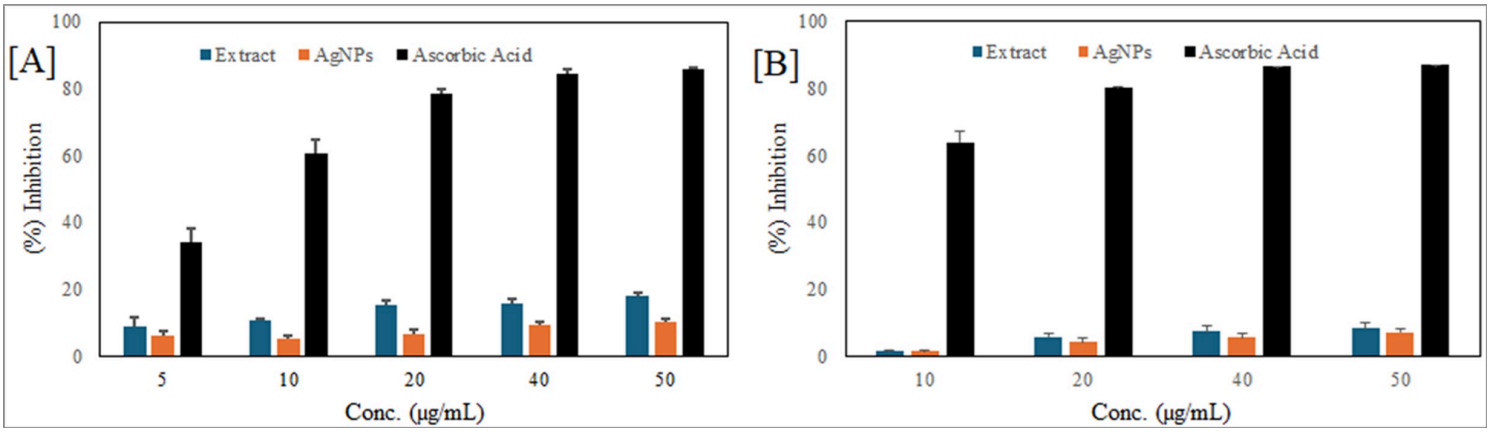

Figure 6

Antioxidant activity of the biosynthesized AgNPs analyzed by DPPH assay. (A) Methanolic extract and Met-AgNPs; (B) Ethanolic extract and Eth-AgNPs.

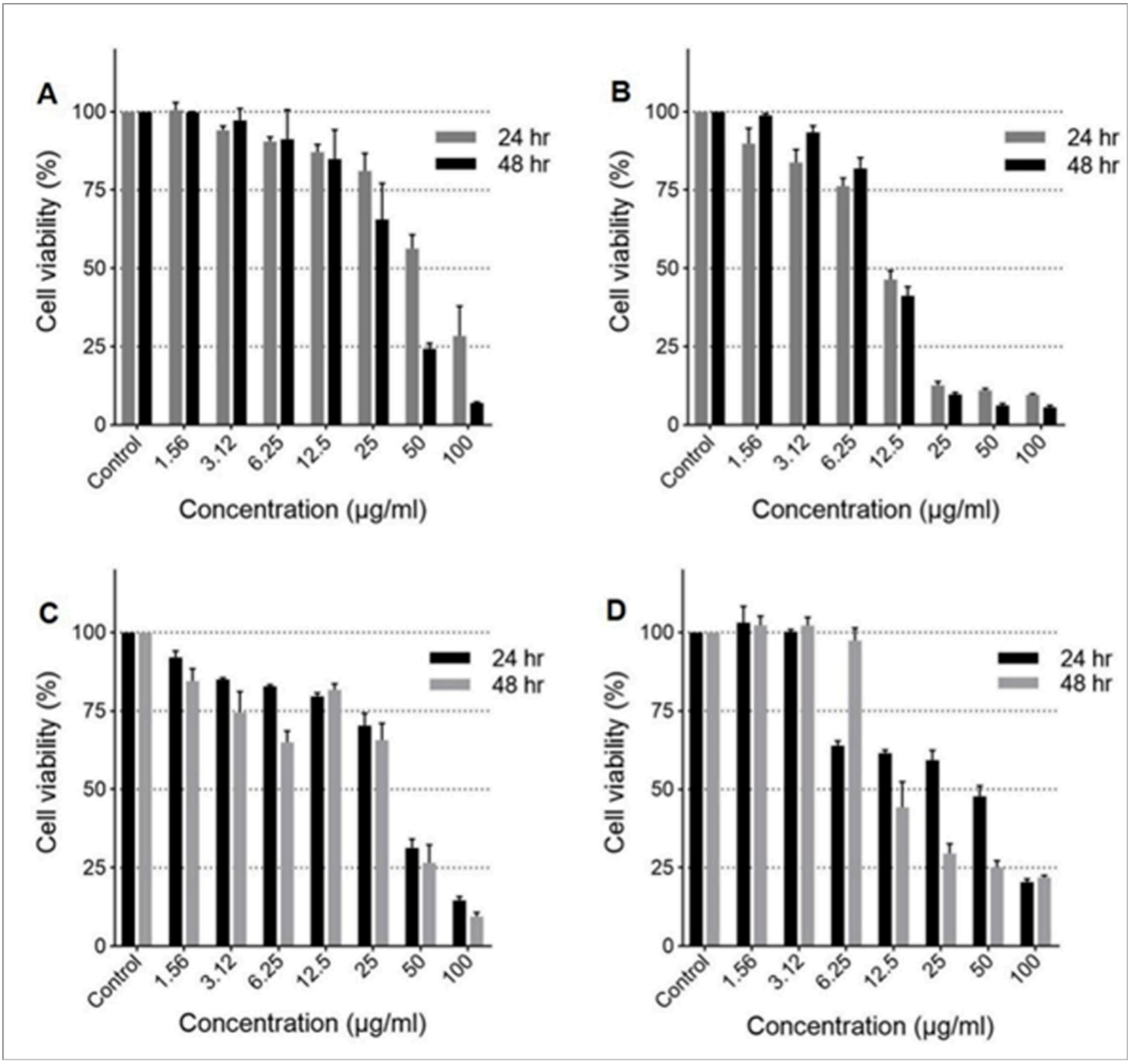

Figure 7

The anticancer activity of synthesized AgNPs was monitored against the MCF-7 and MDA-MB-231 breast cancer cells. The cells were treated with different concentrations (1.56–100 µg/ml) of synthesized AgNPs and cytotoxicity was determined by the SRB method after 24 and 48 hr of incubation. (A) Met-AgNPs effect on MCF-7 cells; (B) Eth-AgNPs effect on MCF-7 cells; (C) Met-AgNPs effect on MDA-MB-231 cells; (D) Eth-AgNPs effect on MDA-MB-231 cells.

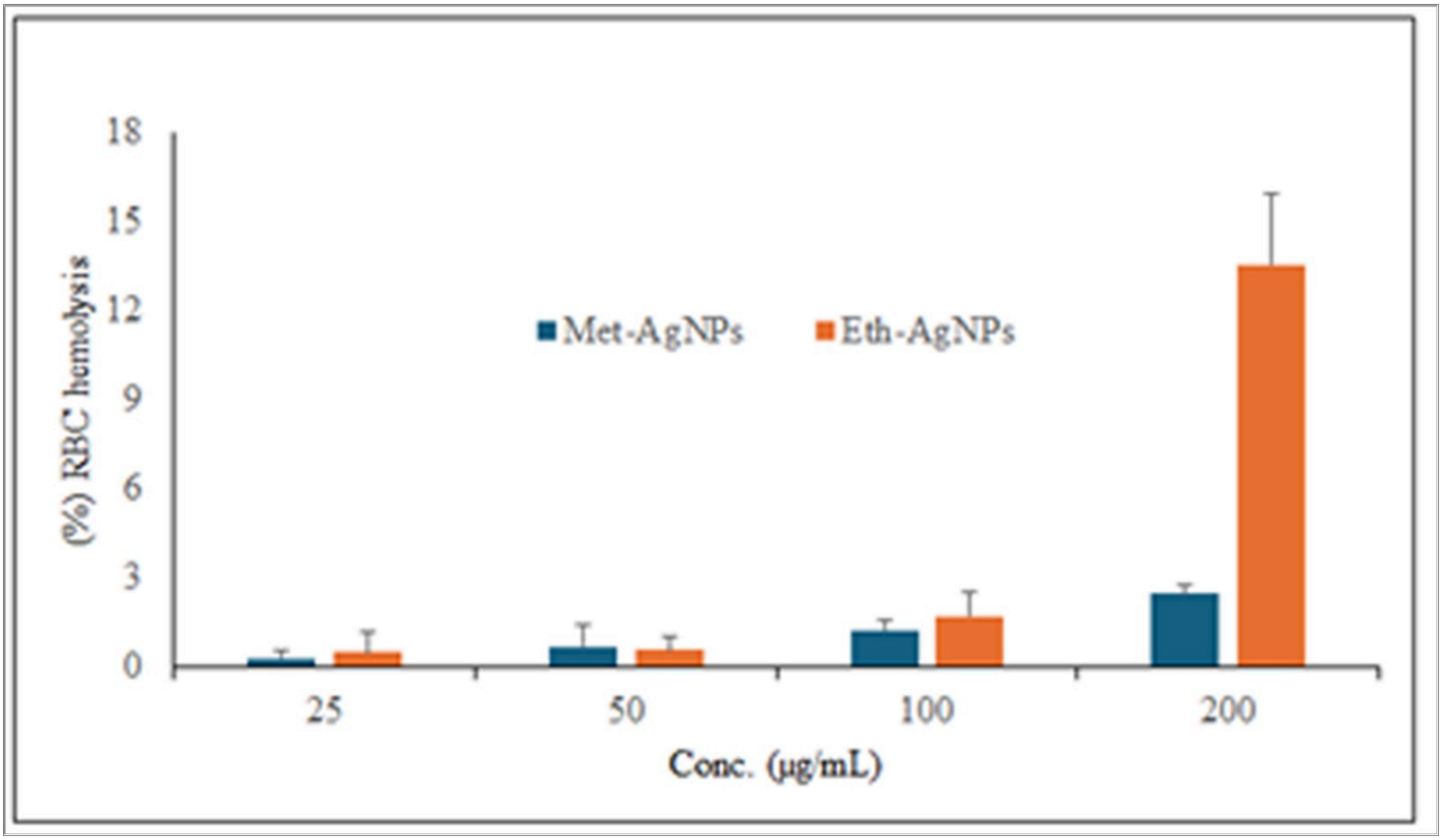

Figure 8

RBC haemolysis (%) activity of the AgNPs treated for 1 hr of methanolic and ethanolic extract-based AgNPs.

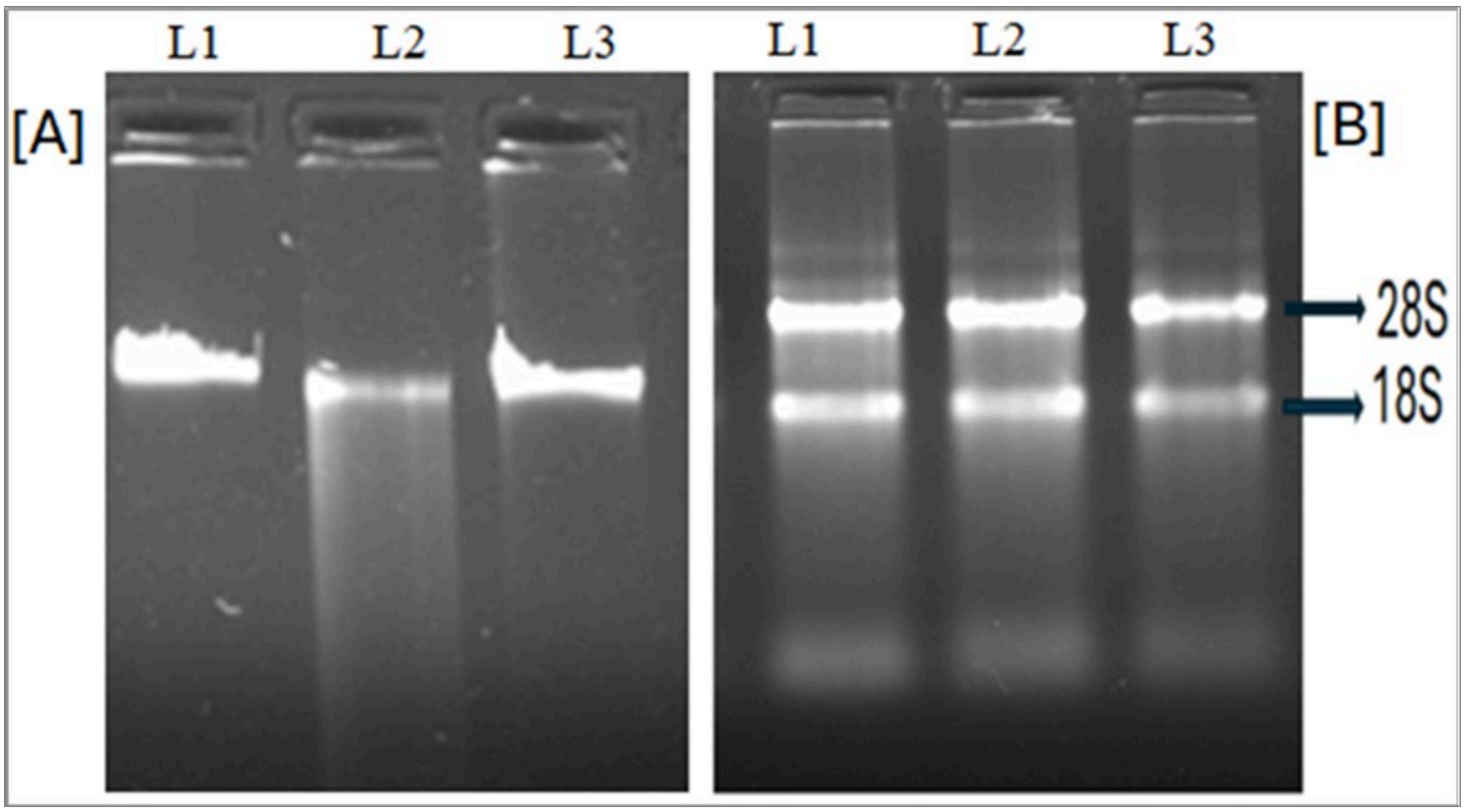

Figure 9

DNA fragmentation study of the MCF cells treated with L1- Control; L2-Eth-AgNPs; L3-Met-AgNPs (A). The image of RNA extracted from the MCF-7 cells treated with AgNPs on 1.2% agarose gel; L1: - Control; L2-: Eth- AgNPs; L3- Met-AgNPs (B).

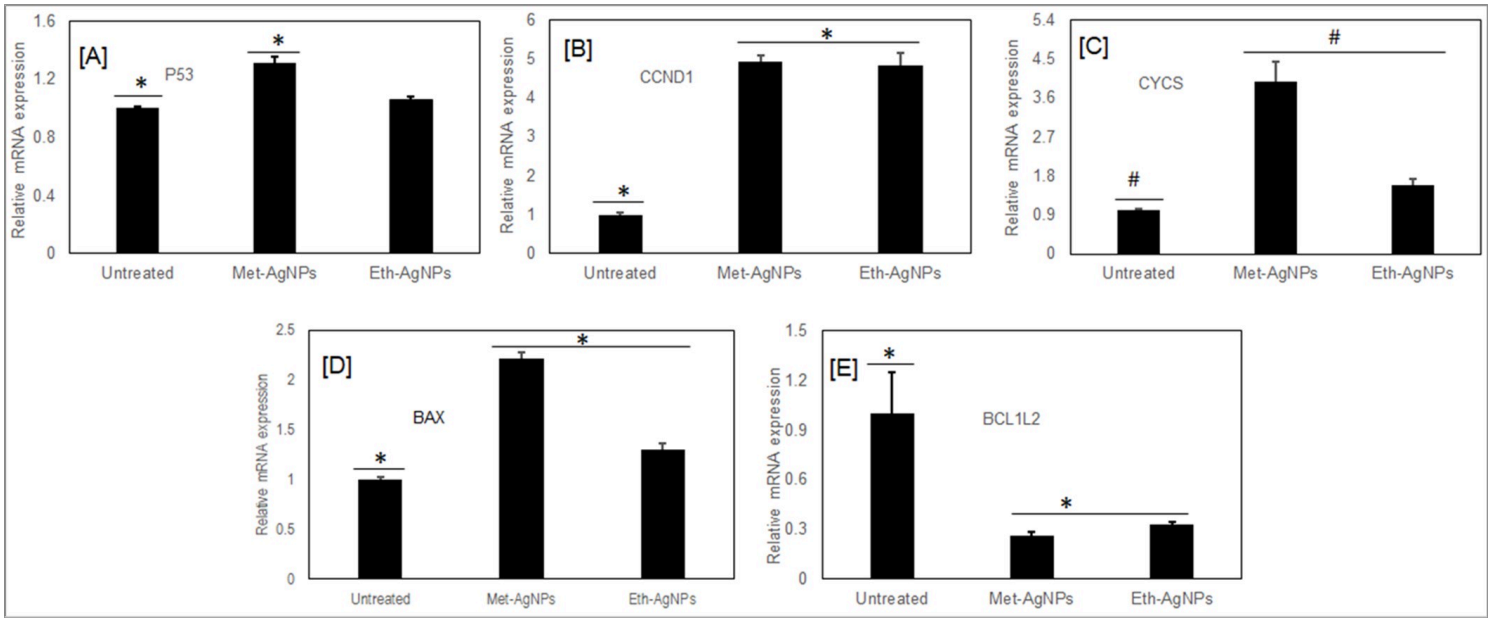

Figure 10

Fig. 10A. Relative mRNA expression of genes of MCF-7 cancer cell lines treated with either Met-AgNPs or Eth-AgNPs. (A) *TP53* gene expression, *p*-value between Untreated *vs.*Meth-AgNPs <0.05; (B) *CCDN1* gene expression, *p*-value Untreated *vs.* Meth-AgNPs <0.05; Untreated *vs.* Eth-AgNPs <0.05. (C) *CYCS* gene expression, *p*-value Untreated *vs.* Meth-AgNPs < 0.05, Untreated *vs.* Eth-AgNPs <0.05. (D). (E) *BAX* gene expression, *p*-value between Untreated *vs.* Met-AgNPs <0.05 and Untreated *vs.*Eth-AgNPs <0.05. (E) *BCL2L1* gene expression, *p*-values Untreated *vs.* Meth-AgNPs <0.05, Untreated *vs.* Eth-AgNPs <0.05.

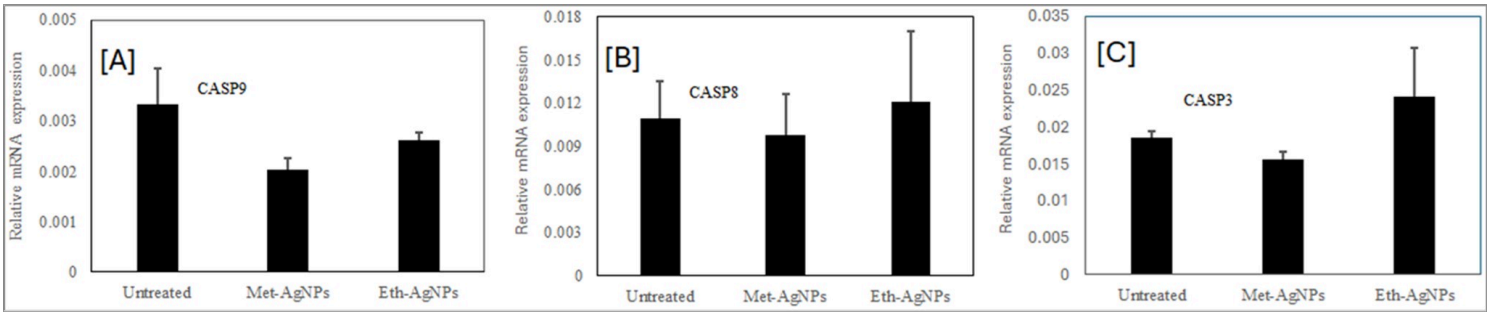

Figure 11

Fig. 10B. Relative mRNA expression of genes *CASP9* (A), *CASP8* (B) and *CASP3*(C) of the MCF-7 cells treated with either Met-AgNPs or Eth-AgNPs. The *p-values*are statistically not significant between groups.

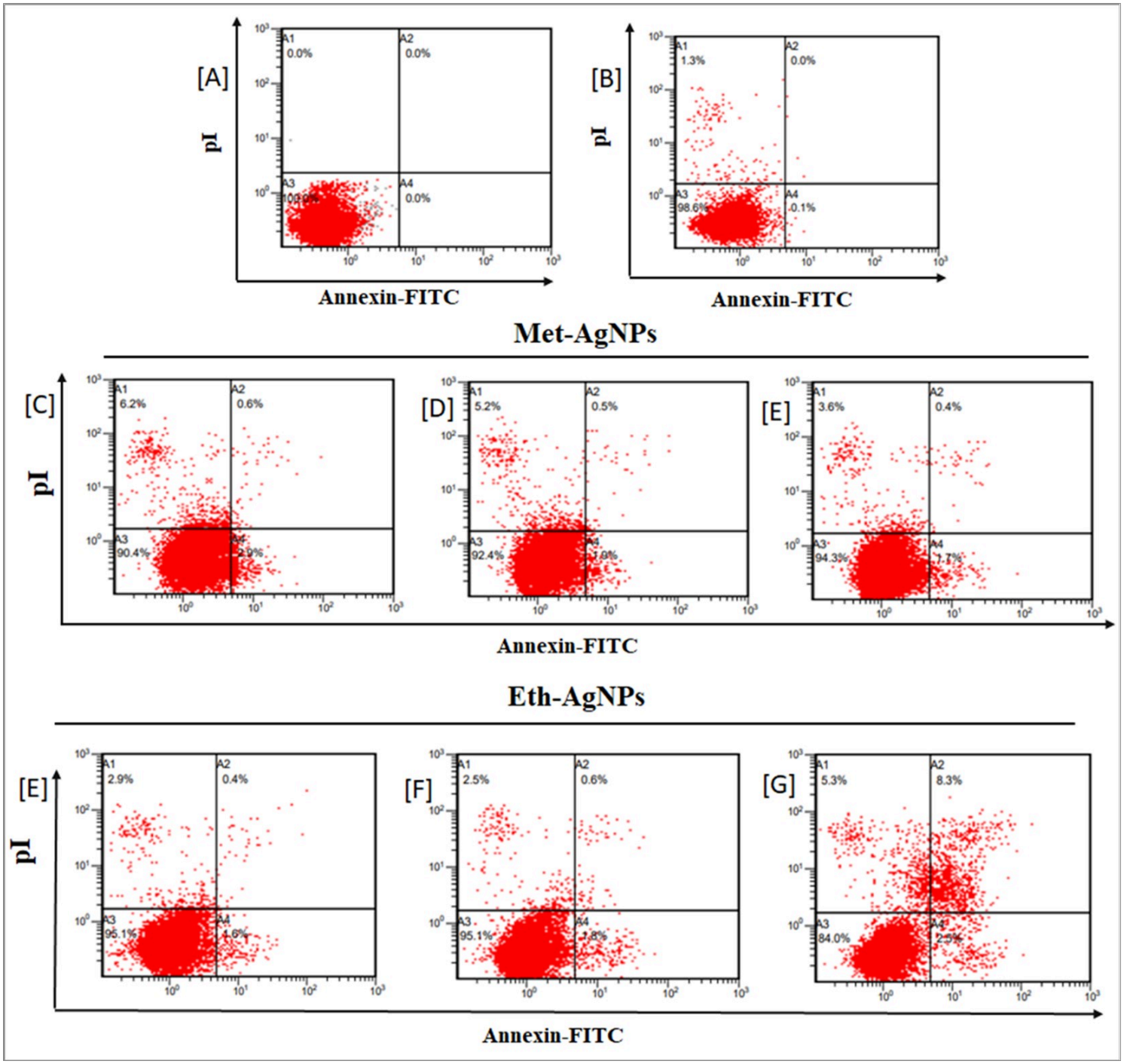

Figure 12

Fig. 11. Flow cytometry analysis of apoptosis induced by different concentrations of Met-AgNPs or Eth-AgNPs. [A] Unstrained cells; [B] Control; [C] 5 µg/mL, [D]10 µg/mL, [E] 25 µg/mL Met-AgNPs; [E] 5 µg/mL, [F] 10 µg/mL, and [G] 25 µg/mL Eth-AgNPs.

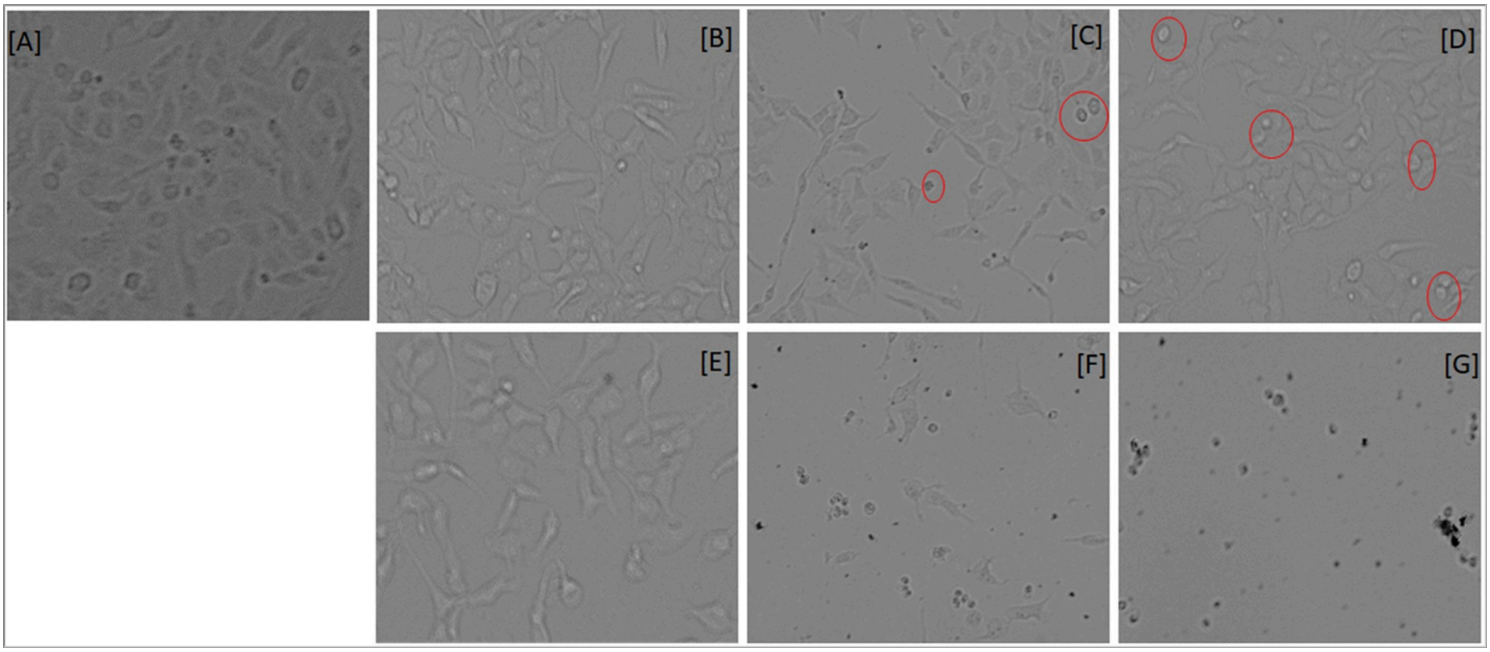

Figure 13

Fig 12. Evaluation of morphological changes of MCF-7 cells (10X) after treatment with different concentrations of AgNPs. [A] Untreated MCF-7 cells; [B] 5 µg/mL Eth-AgNPs; [C] 10 µg/mL Eth-AgNPs; [D] 25 µg/mL Eth-AgNPs; [E] 5 µg/mL Met-AgNPs; [F] 10 µg/mL Met-AgNPs; [G] 25 µg/mL Met-AgNPs.

Supplementary Files

This is a list of supplementary files associated with this preprint. Click to download.

- GA.png